SEISMIC FRAGILITY OF BUILDINGS DAMAGED BY PAST EARTHQUAKES

BY

XINYUAN YANG

THESIS

Submitted in partial fulfillment of the requirements
for the degree of Master of Science in Civil Engineering
in the Graduate College of the
University of Illinois at Urbana-Champaign, 2013

Urbana, Illinois

Adviser:

Professor Paolo Gardoni

ABSTRACT

Fragility analysis plays an important role in seismic risk assessment. Current fragility models of buildings are mostly focusing on the as-built condition of the structure while ignoring the possibility of having multiple earthquakes during the service life of the structure. However, considering the relatively high probability of multiple earthquakes (including main shock-aftershock sequence) and the reality that some buildings might not satisfy the previous seismic design requirement anymore, it is important to include the effect of past earthquakes in fragility estimation of buildings.

In this research, the degradation of important pushover properties of structural columns is applied to represent the damage caused by a past earthquake and new deformation capacity will also be obtained using static pushover analysis. New fragility estimates are conducted to give the fragility of buildings already damaged by earthquakes. By using this mythology, the effect of past earthquakes are included and the new fragility curves can give a more accurate fragility estimate for low rise reinforced concrete building during its service life. This method can be helpful to the decision making process after earthquake hits.

ACKNOWLEDGEMENT

I would like to express profound gratitude to my advisor, Dr. Paolo Gardoni, Associate Professor at the Department of Civil and Environmental Engineering in the University of Illinois, Urbana-Champaign for providing guidance for my research of this thesis.

I sincerely thank all the professors that gave me courses here at the University of Illinois which helps me to become a better civil engineer and those courses will be beneficial in my future career in the field of civil engineering.

I thank my friends and colleagues during my graduate study that help me and encourage me in my study as well as in my life. Everything becomes easier with your help.

Finally, I would also thank my parents for their financial and mental support during my graduate study. It was their encouragement and inspiration that helps me to work hard in my study and get the degree.

TABLE OF CONTENTS

CHAPTER 1
INTRODUCTION

1.1Background

In seismic active zones, buildings are exposed to a relatively high risk of earthquakes and are very likely to be damaged by a main shock-aftershock sequence or multiple earthquakes in the service life. A typical example is the Christchurch earthquake in New Zealand in which an Mw 6.1 earthquake in February 2011 caused extensive damage to buildings damaged by the Mw 7.0 earthquake in September 2010. In the most recent Ya'an earthquake in Sichuan (2013/04/20) , the Mw 7.0 main shock was followed by 712 aftershocks in 12 hours including 2 over Mw 5.0. Current seismic design of buildings is on the basis of one-time performance in its as-built condition while ignoring the possibility that one building might experience more than one earthquake in its service life. However, the risk associated with the damage will increase if the building is already damaged by a past earthquake and its performance might not satisfy the requirement for future earthquakes. In order to provide assessment of the performance and reliability of buildings subject to multiple earthquake events, this study focused on the development of fragility models based on intact and damaged buildings respectively.

In most areas around the world, building damage is the main source of seismic losses when earthquake hits and the buildings designed before the introduction of the seismic resistance design concept might have a relatively higher risk of being damaged. Therefore, estimation of the seismic performance of these buildings will provide some practical reference for reducing earthquake loss which will also be included in this study.

Fragility is defined as a member or system's conditional probability of exceeding a certain limit state under given demand variables and a lot of researches have been done developing the fragility models of building systems (eg. Hwang and Huo 1994; Shinozuka et al. 2000; Wen and Ellingwood 2003; and Ramamoorthy, Gardoni and Bracci 2006). Fragility models of both steel and concrete structures are studied by past researchers while the majority of the models focus on the reliability of the buildings in as-built condition.

Only limited number of researches have been done in the past aiming at understanding the effect of main shock-aftershock sequences or multiple earthquake events on the seismic performance of steel and RC buildings (eg. Lee and Foutch, 2004; Li and Ellingwood, 2007; and Hatzigeorgiou and Liolios, 2010). Luco et al. (2004) proposed a methodology to compute the probabilistic residual capacity of main shock damaged buildings in terms of the ground motion intensity of an aftershock. However, those researches focused on either the demand or capacity side without proposing an overall mythology of seismic fragility estimation for buildings. Kumar and Gardoni (2012) have come up with a seismic degradation reliability model of RC bridges subject to multiple earthquakes and a general stochastic model that can be used to model the deterioration process in engineering systems.

1.2 Objective and mythology

In this thesis, the overall objective is to develop a mythology for analyzing the change of fragility of multi-story reinforced concrete (RC) buildings subject to multiple earthquake events during the service life and the main focus is using an appropriate degradation model for the structures damaged in the past shock.

To achieving the objective, the probabilistic degradation model of RC columns proposed by Kumar and Gardoni (2012) is used to calculate the degradation of static pushover properties of the building damaged by the first earthquake. In order to apply the model to the entire building, the degradation of each column will be calculated separately and then the building will then be analyzed as a whole. In the research, the fragility curve is obtained using virtual experiments conducted by Finite Element software ZUES-NL and a large number of nonlinear time history analysis will be conducted to obtain sufficient data for the proper demand models.

In order to construct the fragility curve of both intact and damaged buildings, the approximation equation developed by Wen et al. is used in which a lognormal distribution of seismic demand and structural capacity is assumed. The demand model is built following the mythology developed by Gardoni et al. (2002). For the deformation capacity, both FEMA performance levels and pushover performance levels will be used. The fragility curves for both intact and damaged structures are constructed by the mythology proposed Ramamoorthy, Gardoni and Bracci (2006) for low-rise RC buildings. In addition, the story specific demand model developed following the mythology of Bai, Gardoni and Hueste (2010) will also be used in order to verify the fragility estimation.

1.3 Organization of the thesis

This thesis will have 3 main sections (Section 2 to Section 4) after the introduction section to present the research done on the topic. Another section (Section 5) will present the conclusions, summaries and suggestions for future work of this study.

In Section 2, the probability of having damaging aftershocks (a specific and most common case of multiple earthquake events) is calculated based on the modified Omori's law. In Section 3, the

fragility curves are developed for two kinds of undamaged structures, one is seismic designed and the other is designed for gravity loads only to represent the largely existed pre-code structures around the world. Section 4 introduced the degradation model of RC columns used in the thesis and proposed a mythology to apply it to the entire structure. In addition, the new fragility curves will be obtained and compared with the fragility curves in Section 3. Section 5 is the summary of the research and presented the conclusions.

CHAPTER 2
AFTERSHOCK STATISTICS

2.1 Introduction

A typical and most common example of multiple earthquake effect is the main-shock aftershock sequence since earthquakes are always followed by a series of aftershocks. Sometimes, when the aftershock has a magnitude larger than the main shock, the main shock is then called a foreshock. The sequence of foreshocks, main shocks and aftershocks often occurs during a certain timespan and for a moderate earthquake with the magnitude of 6.0, the timespan is about 1 year. Therefore, it is very possible that a building damaged in the main shock will be damaged again in the aftershocks and due to limited time between the mainshock and aftershock, repair always becomes impossible. Although most of the structural damage is more likely to occur during the main shock period, significant damage is also observed during the aftershocks since the buildings are already damaged and might not satisfy the original design requirement anymore.

According to the research by Shcherbakov et al. (2005), the time, space and magnitude distribution of aftershocks appear to satisfy the following well known stochastic laws.

1. Like all the other earthquakes, the aftershocks satisfy the Gutenberg-Richter (GR) frequency-magnitude relationship. Therefore, the magnitude distribution of aftershocks could be modeled by the GR relation.
2. The difference between the magnitude of the main shock and that of the largest aftershock is approximately a constant independent of the main shock difference according to the Bath's law.

3. The temporal distribution of the occurrence rate of aftershocks is estimated by the modified Omori's law.

In this section, the probability of aftershocks following a main shock is studied using the above probability laws and the example of the California area will be used as a sample study to reveal the relatively large probability of aftershocks following the main shock.

2.2 Probability of aftershocks in a main shock- aftershock sequence

According to the Gutenberg-Richter relation, the magnitude distribution of aftershocks could be modeled as

$$N(M)=A\bullet 10^{-bM} \tag{2-1}$$

where, M is the magnitude while A and b are constants .

The temporal decay of aftershock activity is given by the modified version of Omori's law developed by Utsu (1961)

$$r=\frac{K}{(c+t)^{p}} \tag{2-3}$$

Where, r is the rate of occurrence of aftershocks; t is the time after the main shock; c and p are regional seismic parameters; K is a function of main shock magnitude Mm and aftershock magnitude M. Although some alternative laws have been proposed (Gross and Kisslinger, 1994), the validity of the modified Omori's law has been supported by observational evidence (Shcherbakov, 2005). Therefore, the modified Omori's law is still used for the purpose of this study.

For this research, only aftershocks with magnitudes large enough to cause damage are concerned. On the basis of the modified Omori's law, the rate of arrival λ of aftershocks larger than M after an Mm magnitude main shock can then be written as (Reasenberg and Jones, 1989)

$$\lambda = \frac{10^{a+b(Mm-M)}}{(c+t)^p} \tag{2-4}$$

Where both a and b are regional parameters which could be obtained from the study of a large number of historical data.

The probability of observing n earthquakes in a time span of T can be computed using the time independent Poisson distribution as follows

$$P = \frac{(\lambda T)^n e^{-\lambda t}}{n!} \tag{2-5}$$

Where λ is the rate of arrival of earthquakes with a certain PGA provided by USGS (2009).

Therefore, the probability of the occurrence of aftershocks (one or more) with a magnitude between M1 and M2 in the time range, t1<t<t2 can then be written as follows

$$P(\mathrm{M}_1, \mathrm{M}_2, \mathrm{t}_1, \mathrm{t}_2) = 1 - \exp[\int_{M_1}^{M_2} \int_{t1}^{t2} \lambda(t, M) dt dM] \tag{2-6}$$

2.3 Case study of California region

A main shock is assumed to occur in California region and the probability of aftershocks is then calculated using equation 2-3 through 2-6.

The value for the constant parameters a, b, c and p in equation 2-4 and equation 2-6 for California are given in Table 3-1 by Reasenberg and Jones (1989). These values are calculated based on 62 main shock-aftershock sequences in California.

Table 2.1 Regional Constant Values for California Region

Parameter	a	b	c	p
value	−1.67	0.91	0.05	1.08

On the basis of the values in Table 3.1, the occurrence probability of one or more aftershocks with different magnitude range after various time span of a magnitude 7.0 main shock is calculated by equation 7 and the results were given in Table 2.2 respectively.

Table 2.2 Cumulative Probability of Aftershock Occurrence with Different Magnitudes in Different Time Periods

Magnitude	Time [d]				
	1	5	10	20	60
5	0.8977	0.9615	0.9736	0.9820	0.9869
5.5	0.5402	0.6703	0.7114	0.7456	0.7980
6	0.2210	0.3000	0.3293	0.3560	0.3936
6.5	0.0628	0.0885	0.0985	0.1080	0.1218

It could be found from the Table that the probability of aftershocks larger than magnitude 5.0 is close to 1 in a main shock-aftershock sequence and the probability of aftershocks with 6.0+ magnitude is close to 0.4 in 60 days after the main shock, which is relatively high. Due to the relatively short time span between the main shock and the aftershock, repair becomes almost impossible if a magnitude 6.0+ earthquake hits after the main shock. Therefore, the consideration of aftershocks will be important for the correct assessment of structural fragility.

Based on the research by Kumar and Gardoni (2012), a damaging aftershock is defined as those that have Richter magnitude M_a greater than or equal to M_m-1 in which M_m is the Richter magnitude of the main shock. Therefore, for a magnitude 7.0 main shock, a damaging aftershock will be that with a magnitude of equal to or larger than 6.0. The cumulative density function (CDF)

of occurrence for one or more aftershocks larger than magnitude 6 after a magnitude 7 main shock is calculated and given in Figure 2.1.

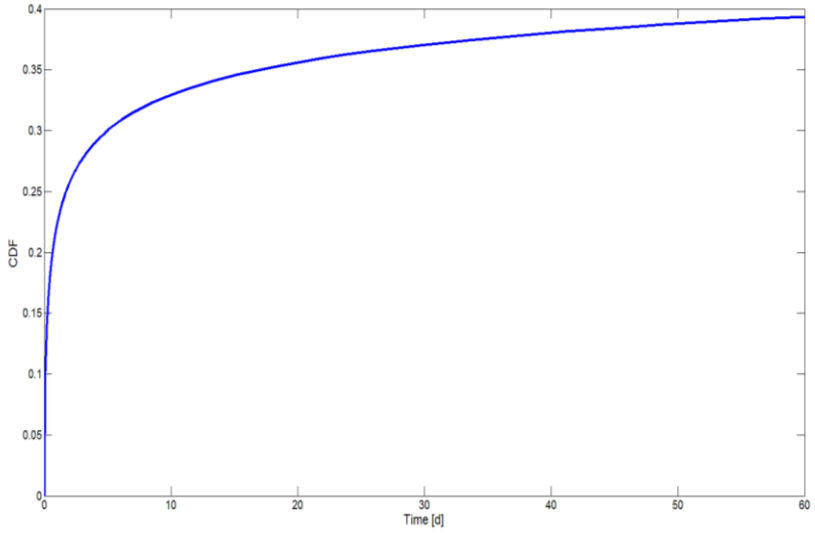

Figure 2.1 Cumulative Density Function (CDF) of M_w 6.0+ Aftershocks in 60 Days after an M_w 7.0 Main Shock

From Figure 3-1 it could be observed that the cumulative probability increases rapidly within the first few days and after 20 days of the main shock, the rate of increasing becomes relatively slow. Therefore, it could be concluded that the damage to structures caused by aftershocks will be more likely to occur right after the main shock which leaves even less time for repair.

Concerning the purpose of this study, aftershock is only a typical example of multiple earthquake since earthquake might hit the same area a longer time after the first earthquake which could not be considered an aftershock since the service of life of a building is much longer comparing to the timespan of main shock-aftershock sequence. Therefore, this study of aftershock statistics actually gives the lower bound for the probability of occurrence of multiple earthquakes during the service life of a building and the actual probability of having multiple earthquakes during the service life could be even higher.

2.4 Conclusions

From the above section, it could be concluded that the probability of damaging aftershocks is relatively large after a relatively large main shock. Since it gives the lower bound for the probability of multiple damaging earthquakes in the same area, the consideration of multiple earthquake events will be important and necessary to estimate the fragility of the building. The fragility based on the consideration of multiple earthquake events will be more accurate than the fragility based on the one time earthquake event considering the as-built condition of the building.

CHAPTER 3
FRAGILITY ANALYSIS OF UNDAMAGED BUILDINGS

3.1 Introduction

Seismic fragility analysis aims at evaluating the performance of structures under earthquake events and it is an important part of risk analysis of buildings. For the development of fragility curves, both capacity limits and demand models are needed.

In this thesis, the mythology proposed by Ramamoorthy, Gardoni and Bracci (2006) is used to construct the fragility model of low rise multi-story RC buildings. A Bayesian mythology is used for developing the demand model based on Gardoni (2002) and the capacity limit states are obtained from FEMA 356. In addition, nonlinear pushover analysis is also performed for obtaining the capacity limit states. In order to obtain a continuous fragility curve, the median estimates of fragility is used. Two sample 2 story reinforced concrete frame buildings were used for the analysis to illustrate the whole analysis process. In addition, the story-specific demand model proposed by Bai, Gardoni and Hueste (2010) will be also used for the fragility estimate and the results will be used to verify the previous results.

3.2 Fragility curve development framework

The brief introduction of the mythology used in this section is presented below.

In this thesis, the earthquake intensity used is spectral acceleration Sa, thus the fragility can be written as the conditional probability

$$F(Sa;\boldsymbol{\Theta}) = P[\mathrm{g(Sa;}\boldsymbol{\Theta}) \le 0 | Sa] \tag{3-1}$$

where g(Sa;$\boldsymbol{\Theta}$) is the limit state function related to both seismic demand and capacity and $\boldsymbol{\Theta}$ is the vector of unknown parameters in the demand model. Based on the research by Bracci et al. (1995), the maximum interstory drift ratio (δ) of frame structures during an earthquake correlates well with the structural damage, thus it was selected in this study to represent the demand of the building.

In this study, the approximation equation developed by Wen et al. is used in which a lognormal distribution of seismic demand and structural capacity is assumed.

$$F(Sa;\boldsymbol{\Theta}) \cong 1 - \Phi\left(\frac{\lambda_c - \lambda_d}{\sqrt{\sigma_D^2 + \sigma_C^2 + \sigma_M^2}}\right) \tag{3-2}$$

where λ_c and λ_d are the mean value of capacity and demand in the lognormal space respectively and σ_D represents the uncertainty associated with the demand model, σ_C represents the uncertainty associated with the capacity model and σ_M represents the modeling uncertainty. In this research, σ_M and σ_C are assumed to be equal to 0.3 according to Wen et al. 2004.

In order to construct the limit state function, both capacity and demand models are needed. The demand model is built following the mythology developed by Gardoni et al. (2002) formulated as

$$D = \ln(\delta) = \theta_0 + \theta_1 \ln(S_a) + \sigma_D \varepsilon \tag{3-3}$$

Where θ_0 and θ_1 are unknown parameters and $\sigma_D\varepsilon$ represents the modal error. According to homoskedasticity assumption, the model variance σ^2_D is independent of Sa. In addition, ε is normally distributed with the mean value of 0 and variance of 1. In this formulation, the aleatory uncertainty is present in Sa and partly in ε while the epistemic uncertainty is present in the model parameters θ_0, θ_1 and σ_D and partly in ε.

Specifically, the bilinear model proposed by Gardoni et al. (2002) is used and equation 3-3 can then be rewritten as

$$\begin{aligned} D_1(S_a;\boldsymbol{\Theta}_1) &= \ln(\delta) = \theta_{10} + \theta_{11}\ln(S_a) + \sigma_{D1}\varepsilon_1; S_a \le \theta_{S_a} \\ D_2(S_a;\boldsymbol{\Theta}_2) &= \ln(\delta) = (\theta_{10} + \theta_{11}\times\theta_{S_a}) + \theta_{21}[\ln(S_a) - \theta_{S_a}] + \sigma_{D2}\varepsilon_2; S_a > \theta_{S_a} \end{aligned} \quad (3\text{-}4)$$

3.3 Structural configuration and design

Even in seismic active zones, some buildings are not designed for seismic loads for various reasons. One reason is those structures were designed in the pre-code era since the concepts of earthquake resistance for buildings have been introduced into the design codes of many countries as late as the 1980s. Another possible reason is that in many developing countries, many structures are designed failing to meet some of the requirements of the relevant design codes. For the purpose of evaluating and comparing the behavior of buildings designed with or without the consideration of earthquake loading, two 2 story reinforced concrete (RC) sample buildings are designed. One building is designed for gravity loads only and the other is designed for both gravity and seismic loads. It could be noted that this building type of low rise framed building is common in most part of the world which could well represent the majority of RC buildings in most seismic active zones.

The first two story reinforced concrete frame building (Structure 1) is designed according to ACI 318-11 for gravity loads only. The design load is a combination of self-weight and 958 Pa superimposed dead load for electrical, mechanical, plumbing and floor and ceiling fixtures; 3650N/m for exterior cladding and 2.4kPa for live loads of a typical office building. It could be noted that the columns of the structure are weaker than the adjoining beams which will lead to the failure mode of column yielding of the structure under earthquake loads. The details of structural

configuration and sections are shown in Figure 3.1.

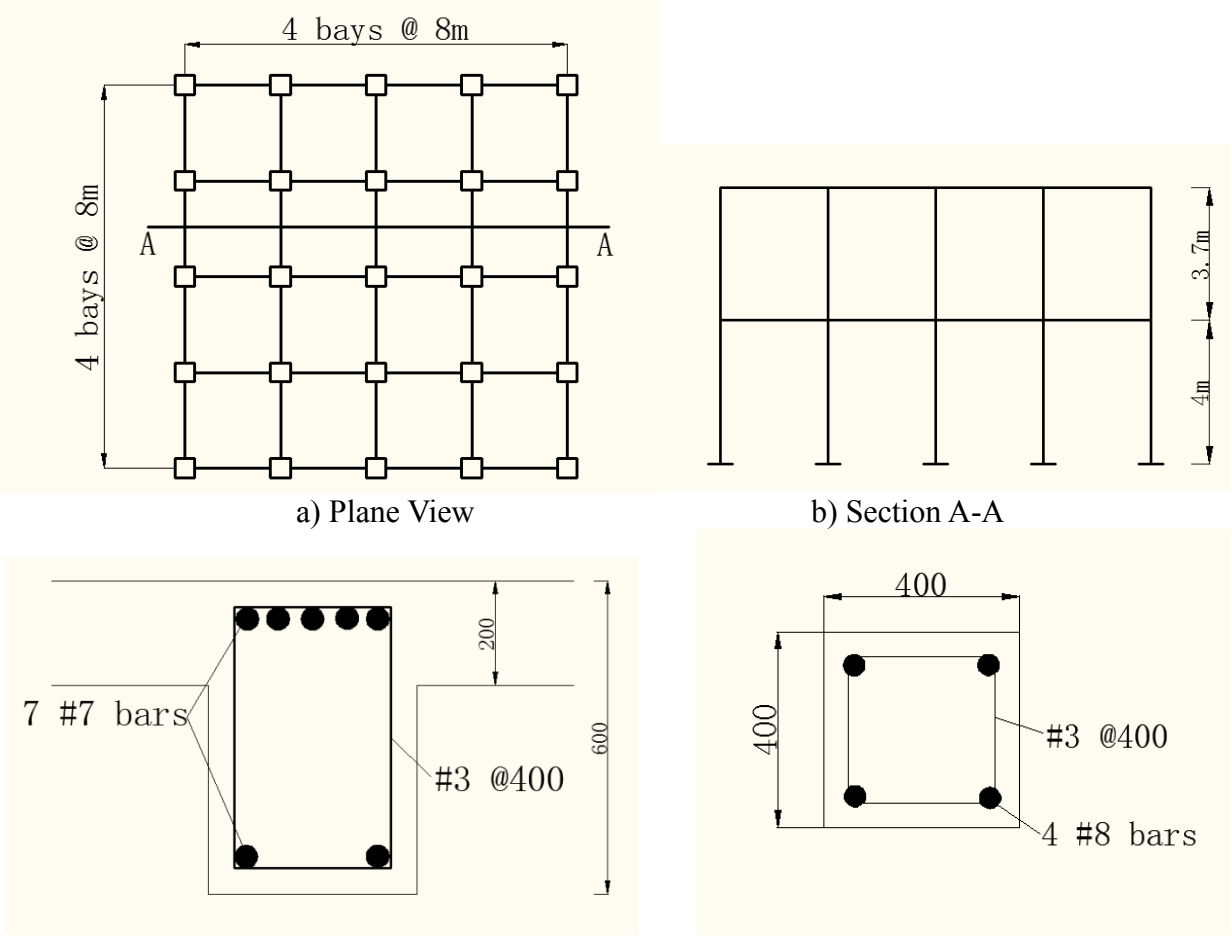

Figure 3.1 Details of Example Structure Designed with Gravity Load Only

Another structure (Structure 2) is designed based on the combination load effect of seismic load and static vertical loads. This seismic design is based on ACI 318 and International Building Code (IBC) 2009. Equivalent lateral force method is used for the seismic design since the structure is both regular and low-rise and the gravity load is the same as the first building. The details of the design of the structure is given in Figure 3.2 (the plan view and section A-A are the same as Structure 1).

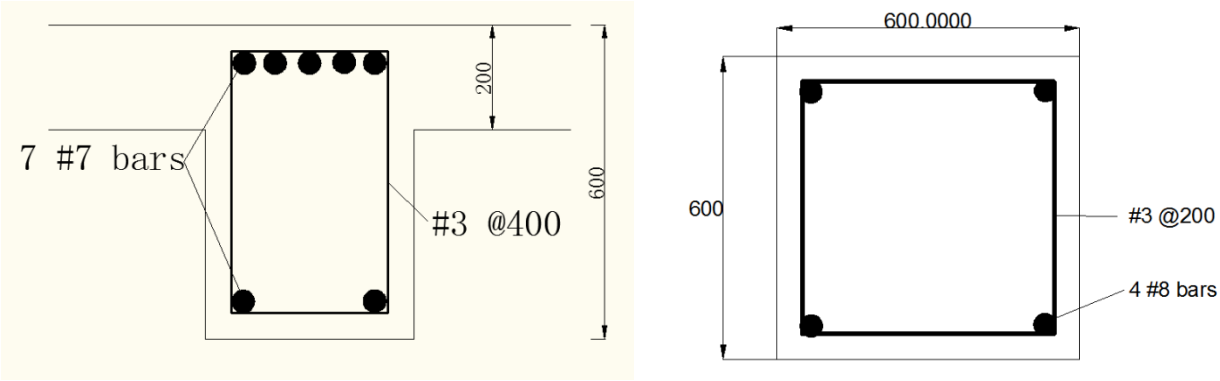

Figure 3.2 Details of Example Structure Designed Considering Seismic Load

A finite element model of the structure is modeled using the non-linear finite element software ZUES-NL. For the materials used, a bilinear elasto-plastic model is used for the steel with strain hardening rate set as 0.005 and the yield strength and Young's modules are 420 N/mm^2 and 200000 N/mm^2 respectively. A nonlinear constant confinement model is applied on the concrete used with a confinement factor of 1.2 and crushing strain of 0.002 mm/mm. The compressive strength of the concrete is 30 N/mm^2 while the tensile strength is 3.3 N/mm^2 .The constitutive relationships of materials are illustrated in Figure 3.3.

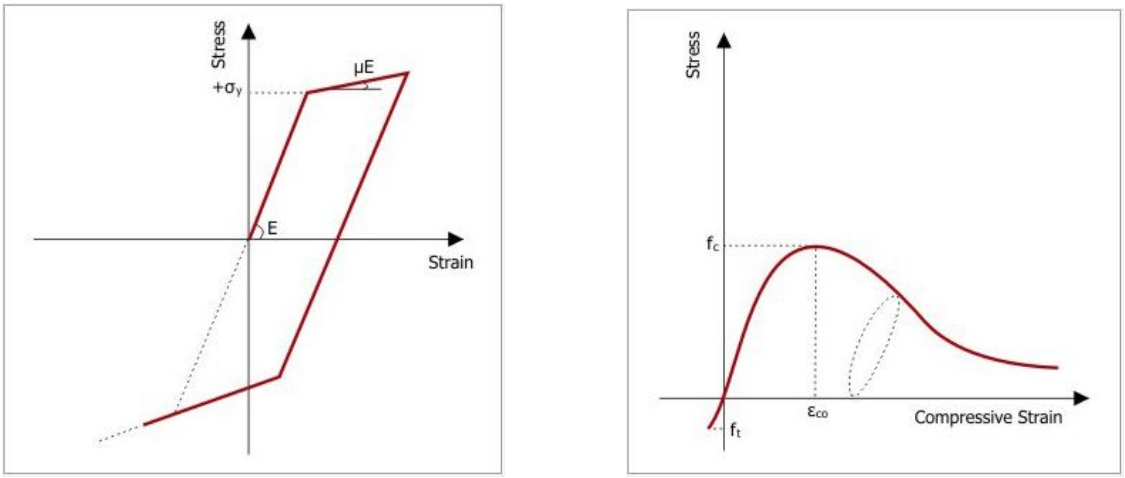

a) Steel model b) concrete model

Figure 3.3 Constitutive Relationship for Materials

Since the building is symmetric, it is modeled as a 2D frame using the nonlinear finite element software ZUES-NL. A lumped mass system is modeled in ZUES-NL for effective computation as illustrated in Figure 3.4.

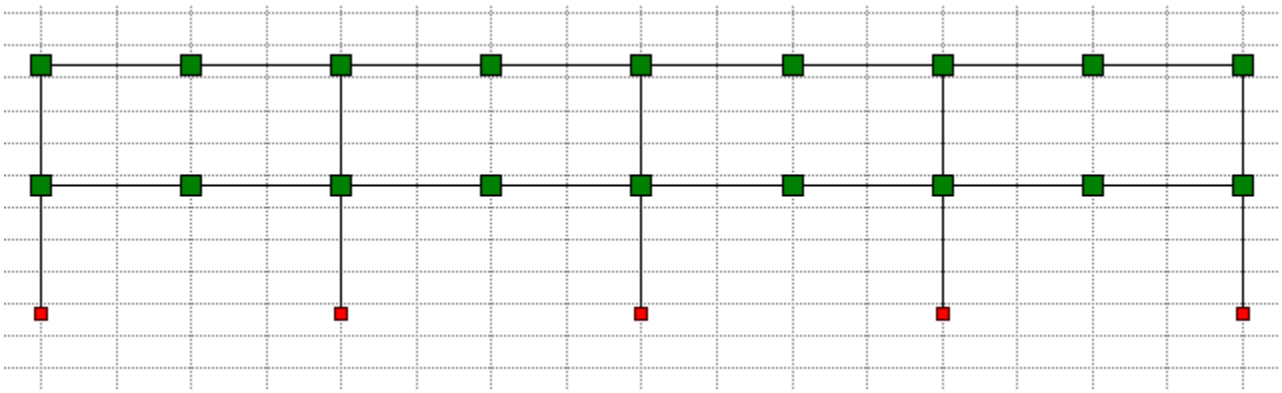

Figure 3.4 Lumped Mass System in ZUES-NL

Eigenvalue analysis of the numerical model is conducted to obtain the important dynamic properties of the structure such as periods and mode shapes. The periods of first three mode shapes of both structures are given in Table 3.1. The shape functions of the first two modes of Structure 1 are illustrated in Figure 3.5 since the shape is similar for both buildings.

Table 3.1 Periods of the First Three Modes of Two Buildings

Modes	1st	2nd	3rd
Structure 1	0.596	0.205	0.148
Structure 2	0.354	0.120	0.111

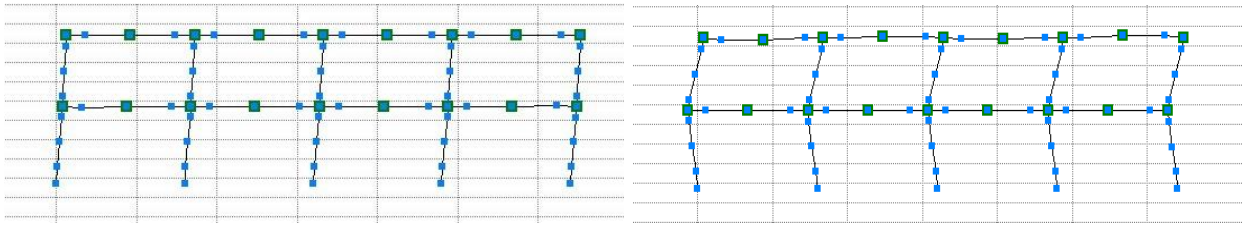

a) Mode 1 b) Mode 2

Figure 3.5 Mode Shapes of the First Two Modes of Structure 1.

From Figure 3-5 it could be concluded that the mode shapes are very close to that of a two degree of freedom system and the third mode is the horizontal mode which contributes little to the overall response of the structure based on the result of the analysis. Therefore, in this study, horizontal earthquake will not be considered aiming at increasing computational efficiency.

3.4 Uncertainties associated with the analysis

In order to derive meaningful models for the fragility relationship, different sources of uncertainty must be accounted for. A systematic framework on uncertainties within earthquake engineering is performed by Wen. et al.(2003) including the aleatory and epistemic uncertainty models that considered system demand and capacity. The uncertainties associated with demand and capacity could be illustrated in Figure 3.6.

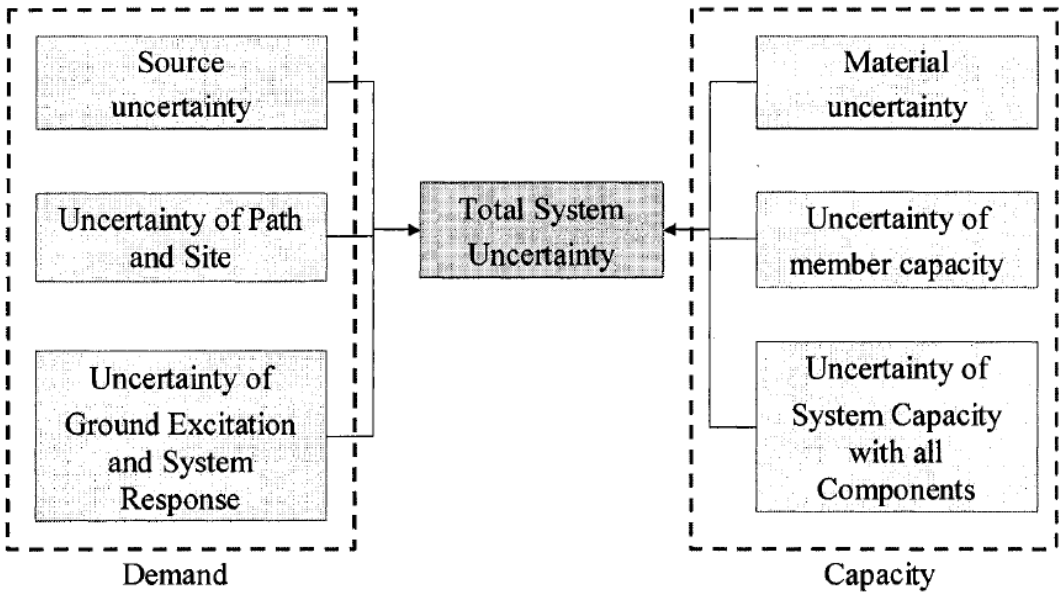

Figure 3.6 Uncertainty Sources for System Demand and Capacity

(Ji.J. and Elnashai, Amr. (2007). Seismic fragility assessment of reinforced concrete high rise buildings. *Doctoral dissertation*, University of Illinois at Urbana-Champaign)

Of all the uncertainty sources, material uncertainty and ground record uncertainty are considered the major uncertainties within the nonlinear time history analysis. In this research, the ground motion uncertainty will be the main source of uncertainty.

In order to assess the seismic demand variables, selecting proper earthquake ground motions for virtual experiments becomes critical. Based on Shome and Cornell(1999), the earthquake ground motion records are divided into five bins based on the moment magnitude and the closest distance from the source R. The first four bins are common earthquake records while the last bin (Bin 5) represents near field ground motion. Near field ground motions are separated from common ground motions due to the reason that they can have unique effect on the structure such as directivity and fling step. The bins selected for this study is indicated in Table 3.2.

Table 3.2 Bins for Selected Ground Motion Records

Bin number	Characteristics	Magnitude	Distance R [km]
1	Large magnitude small distance	M>6.5	[15 30]
2	Large magnitude large distance	M>6.5	[30 50]
3	Small magnitude large distance	M<6.5	[30 50]
4	Small magnitude small distance	M<6.5	[15 30]
5	Near field	M>6.0	[0 15]

All the records are selected from PEER data base and 8 earthquakes are selected for each bin in this study. In order to account for the uncertainty within the ground motion records, the selected records would cover a possibly large range of soil types, magnitudes and seismic mechanisms within each bin. It could also be noted that for each record, horizontal ground motions of both directions are recorded while vertical ground motion is ignored for the purpose of this research. Therefore, 16 ground motion records are selected for each bin and all together 80 records are selected for the purpose of conducting nonlinear time history analysis.

In Table 3.3 to Table 3.7, earthquake records selected for each bin are listed with properties such as magnitude, shear wave velocity (Vs_{30}) closest distance from the source R and peak ground acceleration (PGA).

Table 3.3 Earthquake Records Selected for Bin 1

NO.	Name.	year	station	Vs_{30}[m/s]	M	R[km]	PGA[g]
1	Cape Mendocino	1992	CDMG 89486	457.1	7.0	23.6	0.116
2	CHICHI	1997	ALS	553.4	7.6	15.3	0.183
3	CHICHI	1997	CHY002	235.1	7.6	26.8	0.147
4	Landers	1999	SCE23	271.4	7.3	21.2	0.417
5	Loma Prieta	1989	CDMG58135	714.0	6.9	17.9	0.450
6	KOBE	1995	CUE	312.0	6.9	26.4	0.345
7	Northridge	1994	UCSB78	438.3	6.7	22.2	0.388
8	San Fernando	1971	CDMG128	602.1	6.6	20.3	0.366

Table 3.4 Earthquake Records Selected for Bin 2

NO.	Name.	year	station	Vs30 [m/s]	M	R [km]	PGA [g]
1	Borrego Mtn	1968	USGS117	213.4	6.8	46.0	0.130
2	Cape Mendocino	1992	CDMG 89509	338.5	7.0	44.6	0.178
3	CHICHI	1997	CHY014	473.9	7.6	41.5	0.263
4	CHICHI	1997	CHY015	228.7	7.6	43.5	0.157
5	Kern County	1952	USGS1095	385.4	7.4	41.0	0.178
6	Kocaeli	1999	ERD	424.8	7.4	35.5	0.132
7	Loma Prieta	1989	CDMG 57064	367.6	6.9	43.0	0.124
8	Northridge	1994	USC90079	245.1	6.7	40.7	0.171

Table 3.5 Earthquake Records Selected for Bin 3

NO.	Name.	year	station	Vs30 [m/s]	M	R [km]	PGA [g]
1	Chalfant Valley	1986	CDMG54099	338.5	6.2	44.9	0.071
2	Coalinga	1983	CDMG36230	376.1	6.4	40.5	0.037
3	Imperial Valley	1979	USGS5066	345.4	6.5	49.3	0.128
4	Livermore	1980	CDMG57053	271.4	5.8	37.3	0.073
5	Morgen Hill	1984	CDMG1377	370.8	6.2	30.3	0.044
6	N. Palm Springs	1986	CDMG12331	338.5	6.0	43.3	0.144
7	Whittier Narrows	1987	USC90053	267.5	6.0	47.4	0.139
8	Coyote Lake	1979	CDMG57191	281.6	5.7	31.2	0.050

Table 3.6 Earthquake Records Selected for Bin 4.

NO.	Name.	year	station	Vs30 [m/s]	M	R [km]	PGA [g]
1	Chalfant Valley	1986	CDMG54424	345.4	6.2	23.0	0.165
2	Coyote Lake	1979	CDMG1377	370.8	5.7	15.6	0.108
3	Livermore	1980	CDMG67070	338.5	5.8	20.3	0.051
4	Morgen Hill	1984	CDMG47379	1428.0	6.2	16.2	0.098
5	N. Palm Springs	1986	CDMG22170	379.3	6.0	29.8	0.065
6	Superstitn Hills	1987	USGS5210	207.5	6.3	24.7	0.134
7	Whittier Narrows	1987	USGS951	370.8	6.0	23.3	0.149
8	Coalinga	1983	CDMG36438	376.1	6.4	29.6	0.072

Table 3.7 Earthquake Records Selected for Bin 5

NO.	Name.	year	station	Vs30 [m/s]	M	R [km]	PGA [g]
1	Cape Mendocino	1992	CDMG89005	513.7	7.1	8.5	1.497
2	Chalfant Valley	1986	CDMG54171	271.4	6.2	9.2	0.248
3	CHICHI	1999	CHY028	542.6	7.6	7.3	0.821
4	Coalinga	1983	USGS1162	257.4	6.4	8.5	0.592
5	DUZE	1983	ERD	276.0	7.1	8.2	0.535
6	Imperial Valley	1979	USGS5054	223.0	6.5	2.5	0.775
7	KOBE	1995	CUE	609.0	6.9	11.1	0.509
8	Nahanni	1985	6097	659.6	6.8	6.0	1.096

To better illustrate the difference between the results of each bin and the necessity of conducting this bin selection, spectral acceleration of each bin is calculated and the response spectrums were present in Figure 3.7 to Figure 3.11. It could be noted that the software Seismo Signal is used to obtain the response spectrums and 5% viscous damping is assumed for all ground motion records.

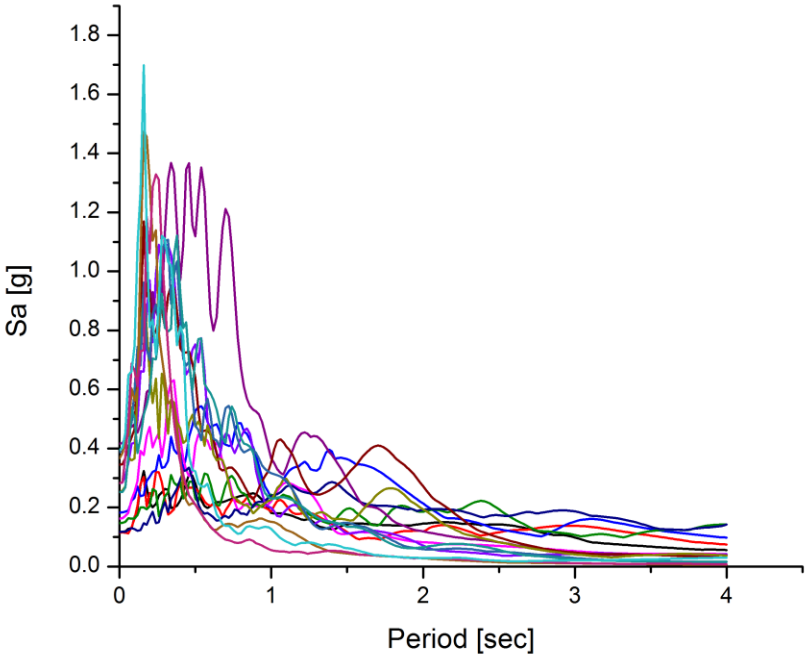

Figure 3.7 Response Spectrum for Bin 1 Ground Motions

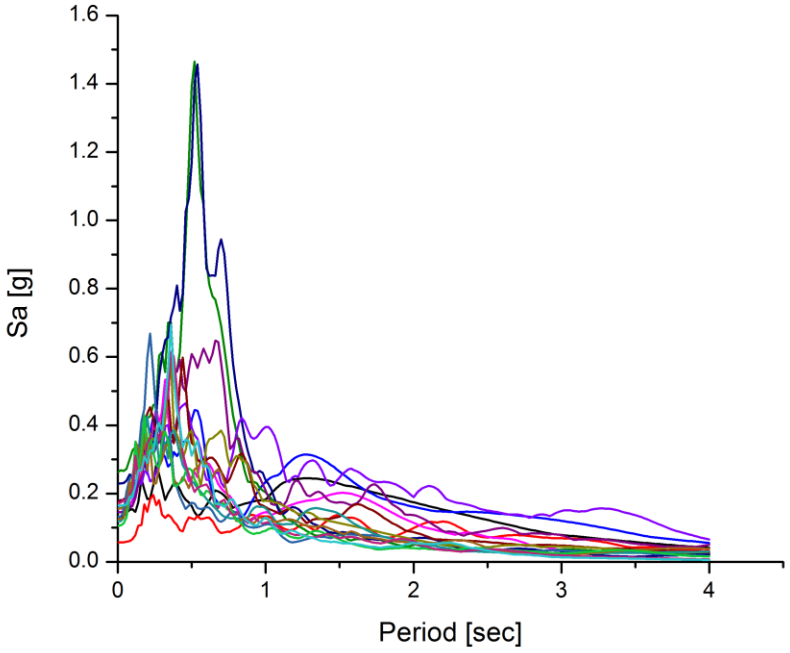

Figure 3.8 Response Spectrum for Bin 2 Ground Motions

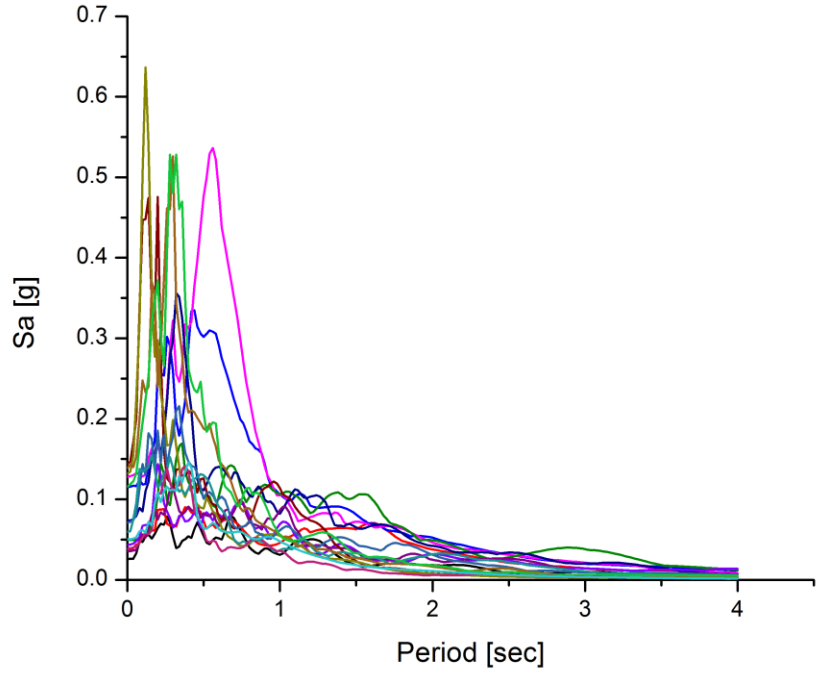

Figure 3.9 Response Spectrum for Bin 3 Ground Motions

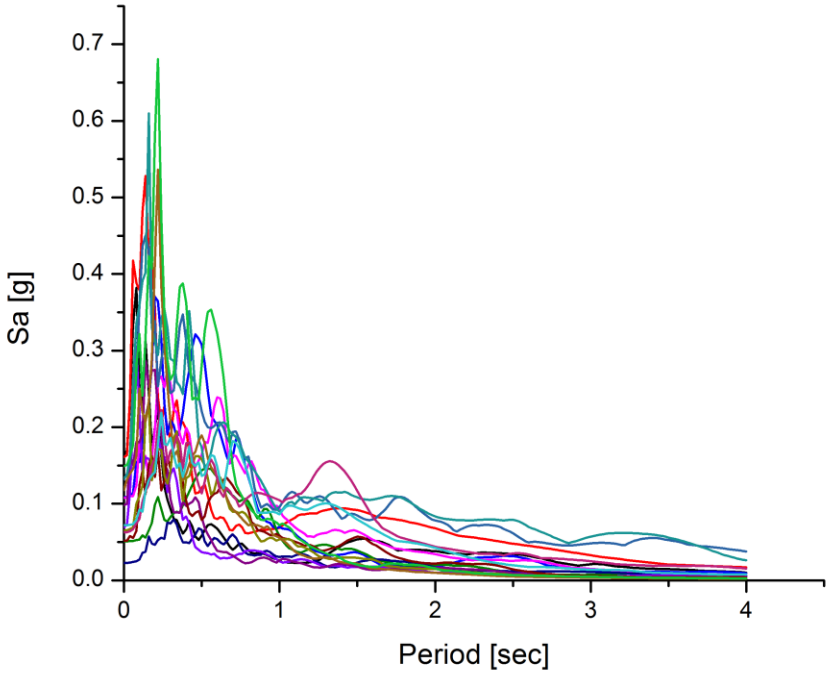

Figure 3.10 Response Spectrum for Bin 4 Ground Motions

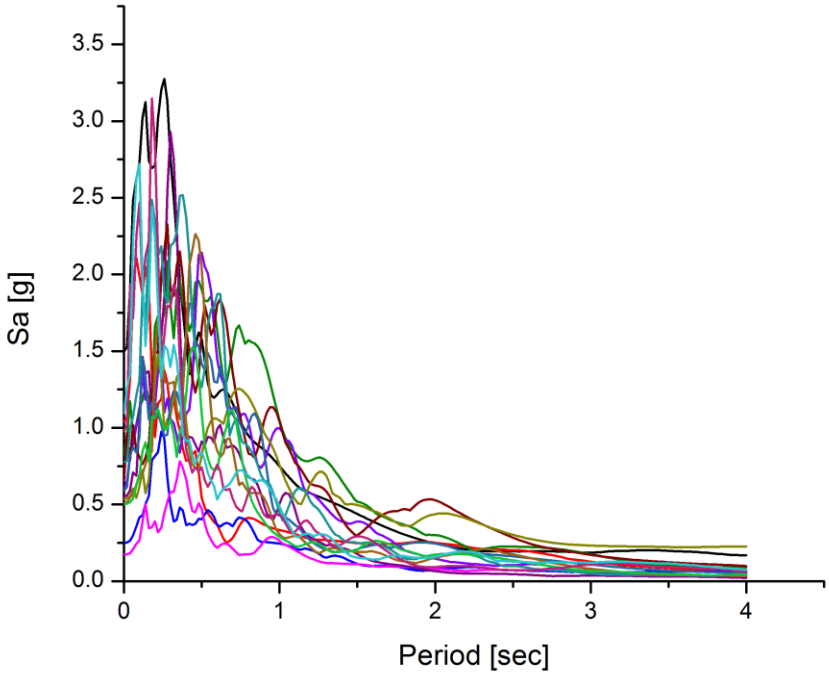

Figure 3.11 Response Spectrum for Bin 5 Ground Motions

From the above figures it could be found that the response spectrum of each bin showed common features as a result of different distance and magnitude. For Bin 1 which is large magnitude small distance, the spectral acceleration exhibited a high peak value and the period corresponding to the peak period was relatively small, under 0.3 second. For Bin 2 which is large magnitude large distance, the peak value of spectral acceleration is still relatively large but the period corresponding to the peak value is considerably larger than Bin 1, around 0.5 second. For Bin 3 and Bin 4, the peak spectral acceleration was smaller while the period corresponding to the peak response increased with the increasing distance. For Bin 5 which corresponds to close site ground motion records, the maximum spectral acceleration is significantly larger than the other four bins which represents the severe ground motion.

For checking the representative of the selected ground motions, the median value of the computed

spectral acceleration (Sa) is compared with the median spectral acceleration (Sa) calculated using the attenuation law of Abramhamson and Silva (1997). For the calculation using the attenuation law, the central values for M and R ranges of each bin are used. The results are shown in Figure 3.12.

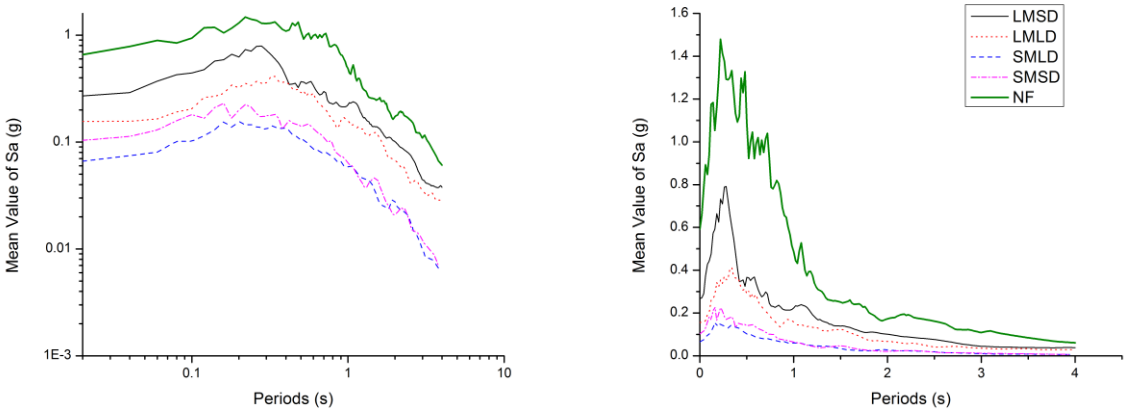

a) Based on selected ground motions for each bin (left: log-log space; right: original space)

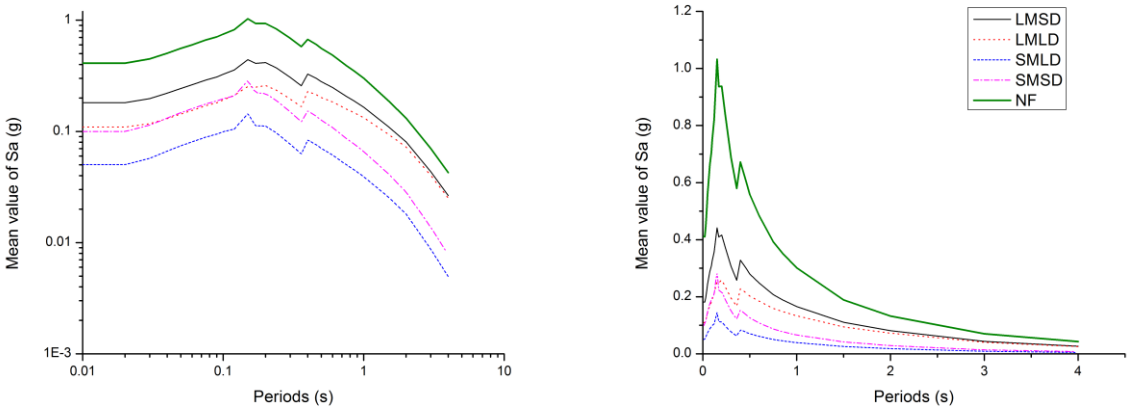

b) Based on attenuation law by Abrahamson and Silva (1997) (left: log-log space; right: original space)

Figure 3.12 Median Spectral Acceleration Spectral for Each Bin with 5% Damping

The variability in the frequency content of the selected ground motion is also checked by

comparing with the attenuation law of Abrahamson and Silva (1997) in a similar way as the median spectral acceleration. The results are shown in Figure 3.13.

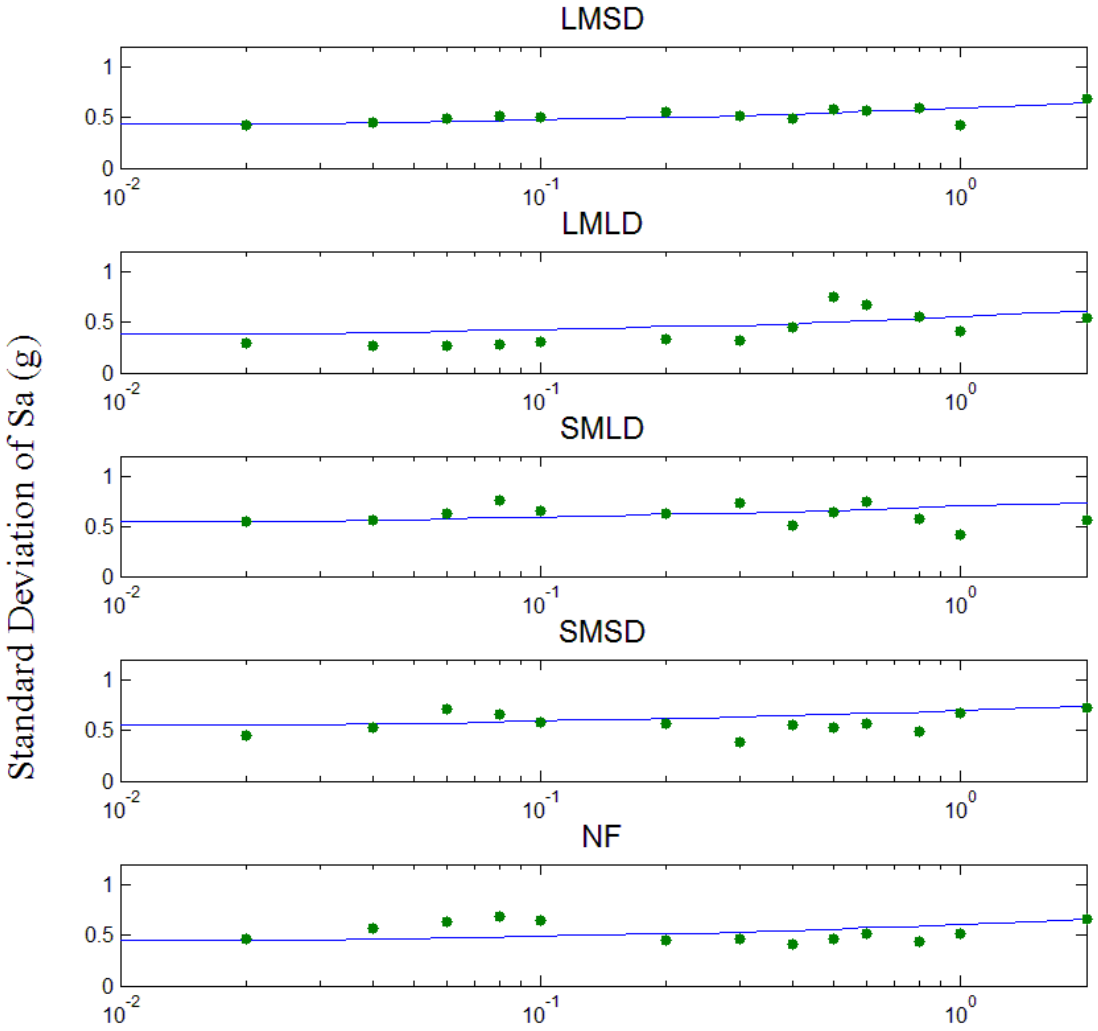

Figure 3.13 Comparison of Standard Deviation of Sa Values Obtained by Ground Motions (Dots) and Standard Deviation Values Based on Attenuation Law by Abramhamson and Silva (1997) (Solid Lines) for Each Bin With 5% Damping

From Figure 3.12 and Figure 3.13 it could be found that the results based on selected ground motions records were very close to the theoretical results calculated using the attenuation law of Abramhamson and Silva (1997), indicating that the selected results were representative enough for the purpose of conducting the fragility analysis.

3.5 Virtual experiments and seismic demand

The probability demand model will be constructed based on a bilinear model proposed by Gardoni et al. (2002) given in equation 3-3 and equation 3-4.

The parameters in equation 3-3 will be updated by the well-known Bayesian updating rule (Box and Tiao, 1992)

$$f(\boldsymbol{\Theta}) = kL(\boldsymbol{\Theta})p(\boldsymbol{\Theta}) \quad (3\text{-}5)$$

Where L is the likelihood function including the objective information of the observations made and p denotes the prior distribution of $\boldsymbol{\Theta}$ reflecting our state of knowledge about the parameter; f is the posterior distribution representing the updated knowledge of $\boldsymbol{\Theta}$ and k is the normalizing factor. This Bayesian updating rule accounts for both aleatory and epistemic uncertainty. The aleatory uncertainty comes from the inherent variability or randomness of the phenomena and the epistemic uncertainty is the result of lack of knowledge, probable model inexactness and statistic uncertainty.

In this study, since a large number of observations would be made based on nonlinear time history analysis, the prior distribution will not have a large influence on the posterior distribution. If the number of observations is small, then the influence of the prior will be dominant.

Virtual experiments were conducted using ZUES-NL. Non-linear time history analysis was performed based on different sets of earthquake ground motion records to obtain enough data for the regression analysis and. Maximum interstory drift ratio δ is selected to be the seismic demand parameter for the development of fragility curves. In Figure 3.14, the plots of ln(δ) versus ln(Sa) for both buildings were shown and for each building, 120 time history analyses were performed and 120 data points were obtained.

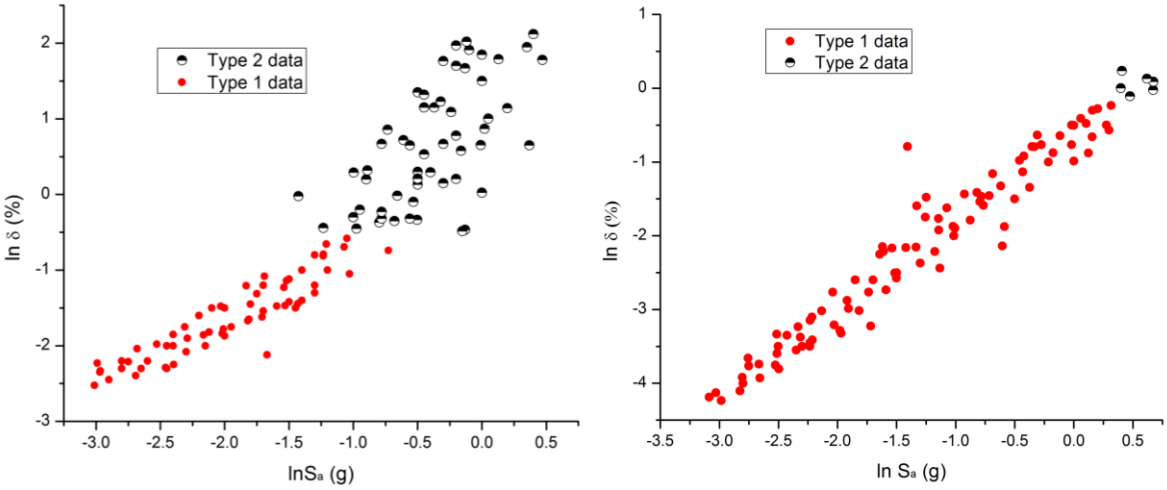

Structure 1 Structure 2

Figure 3.14: Maximum Interstory Drift Ratio Response Data from Nonlinear Time History Analysis

The data are categorized into two different types based on the trends in the data as exhibited in Figure 3.14. The first type (Type 1) data is defined as $\delta < \delta_1$ in which δ1 is 0.62% for Structure 1 and 0.85% for Structure 2 in this research and the elastic response is dominant in the response of Type 1 data due to the relatively smaller value of Sa. Type 2 data is defined as $\delta > \delta_1$ in which inelastic response of the structure makes a large proportion of the response. The values for δ_1 is decided by non-linear pushover analysis and the definition of first yield point is used for the

purpose of this research. It could be found that for Structure 2, almost all the data are Type 1 data since the structure always behaves in the elastic range for the given spectral acceleration values.

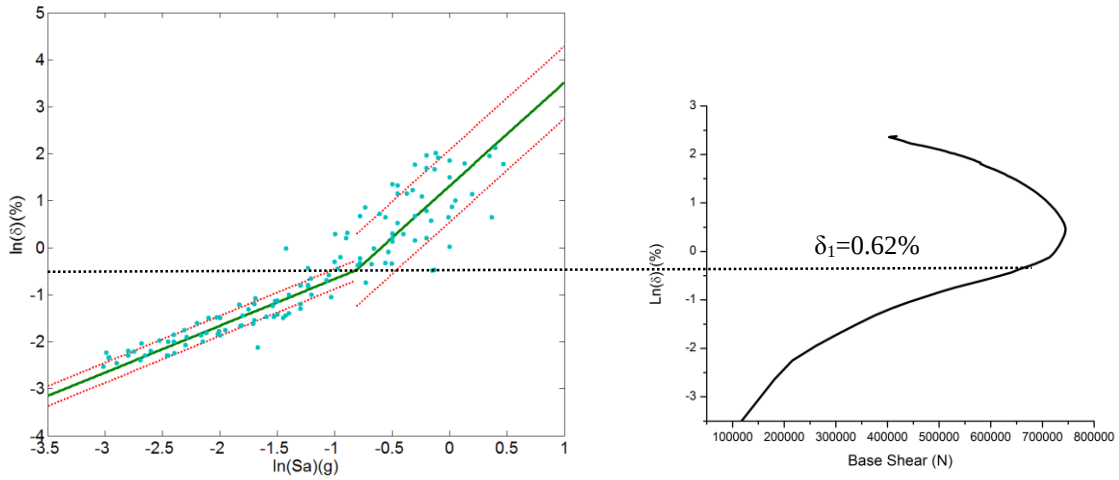

Figure 3.15 Bilinear Demand Model for Structure 1

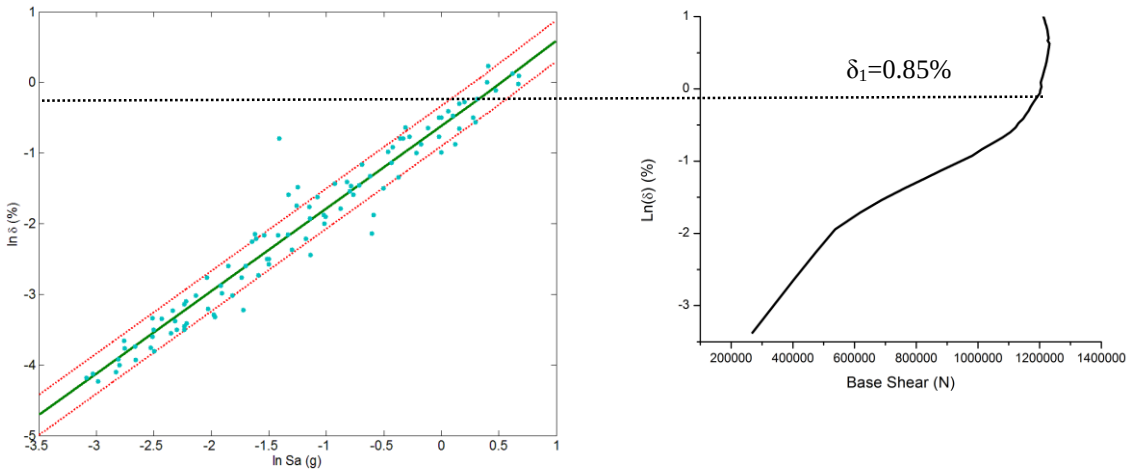

Figure 3.16 Bilinear Demand Model for Structure 2

The bi-linear demand model were used for the regression analysis for both Structure 1 and Structure 2 as shown in Figure 3.15 and Figure 3.16 based on equation 3-3. The solid line on the

left half of Figure 3-13 represents the resulting bi-linear demand model and the dash line represents the range of $\pm\sigma$. The right part of Figure 3-13 is the pushover curve in which the maximum inter-story drift δ is plotted on the log scale. Using this figure, the value for δ_1 is clearly illustrated. For Structure 2, since almost all the data are type 1 data, the bilinear model very be very close to a singer linear model. The posterior parameters after the regression analysis are given in Table 3.8, Table 3.9 and Table 3.10 for both structures.

Table 3.8 Posterior Statistics of the Parameters in the Demand Model

Structure Type		Parameter		
		θ_0	θ_1	σ
Non-Seismic Designed	$\delta < \delta 1$	0.3292	0.9963	0.2130
	$\delta > \delta 1$	1.3091	2.2057	0.7692
Seismic Designed	$\delta < \delta 1$	−0.6213	1.1692	0.2856
	$\delta > \delta 1$	−0.6457	1.2312	0.2913

It could be found from Table 3.8 that for Structure 1, the parameter σ varies significantly for Type 1 and Type 2 data. The reason for that is mainly due to the randomness of ground motions at large intensities. Therefore, the use of a bilinear model could provide a more accurate result than the singer linear model in this case.

Table 3.9 Posterior Statistics of Unknown Parameters in the Demand Model for Non-Seismic Designed Building

Range	Parameter	Mean	Standard deviation	Correlation Coefficient		
				θ_0	θ_1	σ
$\delta < \delta 1$	θ_0	0.3292	0.038	1	0.98	−0..01
	θ_1	0.9963	0.021	0.98	1	0.01
	σ	0.2130	0.007	−0.01	0.01	1
$\delta > \delta 1$	θ_1	2.2057	0.115	NA	1	0.35
	σ	0.7692	0.068	NA	0.35	1

Table 3.10 Posterior Statistics of Unknown Parameters in the Demand Model for Seismic Designed Building

Range	Parameter	Mean	Standard deviation	Correlation Coefficient		
				θ_0	θ_1	σ
$\delta < \delta 1$	θ_0	−0.6213	0.014	1	0.97	−0.01
	θ_1	1.1692	0.032	0.97	1	−0.01
	σ	0.2856	0.008	−0.01	−0.01	1
$\delta > \delta 1$	θ_1	1.2312	0.048	NA	1	0.44
	σ	0.2913	0.004	NA	0.44	1

3.6 Seismic capacity

The capacity limit state plays a vital role in the construction of fragility curves. The ideal way of obtaining the capacity models should be based on previous seismic performance or experimental data. However, since these data are absent, two methods are used to obtain the capacity model. The first one is to use the performance limit states defined in FEMA 356 and the second one is to conduct non-linear pushover analysis.

The performance limit states are well defined in FEMA 356, and for low story RC buildings, the maximum interstory drift limit for Immediate occupancy (IO), Life Safety (LS) and Collapse Prevention (CP) are 1%, 2% and 4% accordingly. The detail description of the different performance limit states is given in Table 3.11.

Table 3.11 Description of Different Performance Levels Based on FEMA 356

Performance Level	Description
IO	Occupants allowed immediate access into the structure following the earthquake and the pre-earthquake design and strength and stiffness are retained.
LS	Building occupants are protected from loss of life with a significant margin against the onset of partial or total structural collapse
CP	Building continues to support gravity loading, but retains no margin against collapse

However, for the structure designed for gravity loads only, the limit state might not be representative since the performance levels are mainly based on structures designed for seismic loads. Therefore, the limit state used in this study for the structure designed for gravity loads only (Structure 1) will be 0.5%, 1% and 2% for the three performance levels accordingly as suggested

by Ramamoorthy et al. (2006). The limit states for Structure 2 will remain the same as the performance levels described in FEMA-356.

In the pushover analysis, horizontal static forces or displacements are applied to lateral action resisting systems. The forces or displacements are distributed along the height of the structure to simulate inertia forces or their effect (Elnashai and Di Sarno 2008). In this study, an inverted triangular distribution of lateral forces is applied to the 2D frames due to the dominance effect of the fundamental mode in the direction under consideration. The results of the pushover analysis for both frames are shown in Figure 3.17.

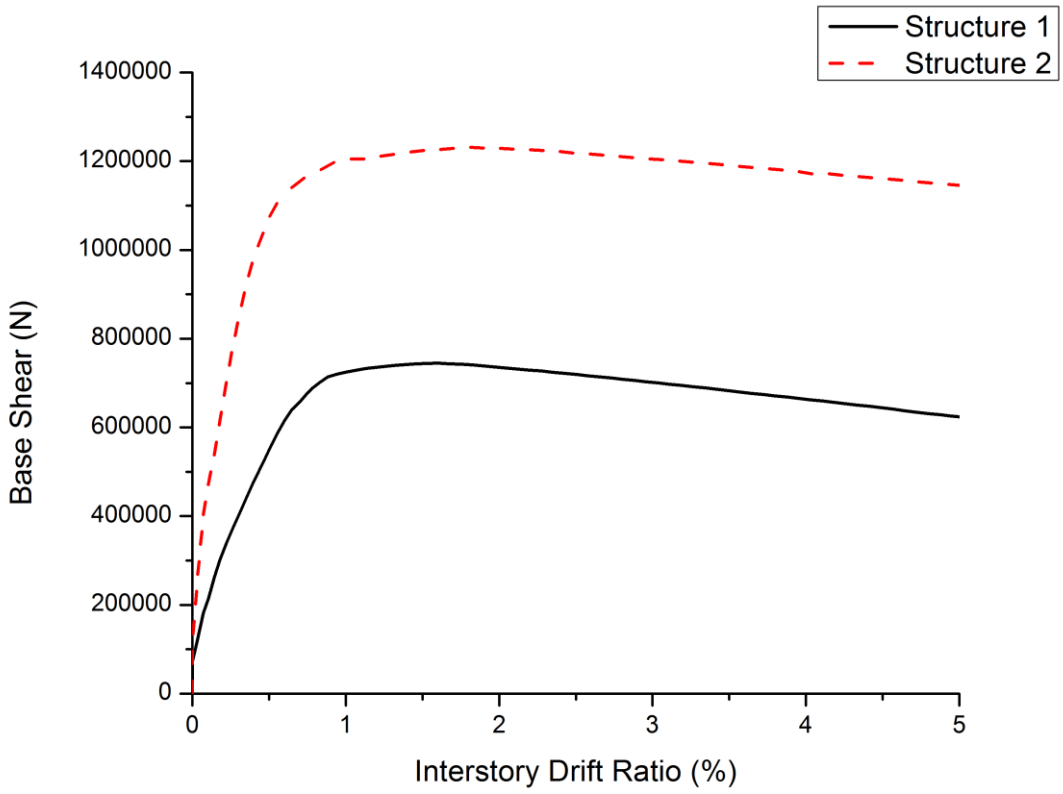

Figure 3.17 Results for Non-linear Pushover Analysis

The yield deformation (YD) is defined as the first yield point and the ultimate deformation (UD) is defined as the apex of the load-displacement curve (Park, 1988). The resulting yield and ultimate deformations for the two structures are given in Table 3.12.

Table 3.12 Yielding and Ultimate Interstory Drift Ratio for Both Buildings

Structure Type	Yielding δ (%)	Ultimate δ (%)
Non-Seismic Designed	0.62	1.60
Seismic Designed	0.85	2.00

It could be concluded from Table 3.12 that the yielding and ultimate δ values for the non-seismic designed building are significantly less than the performance level of 1%, 2% and 4%. They are even less than the reduced values used which are 0.5%, 1% and 2% respectively. Considering the fact that the structure could still deform slightly beyond the ultimate deformation defined in this case, it will be proper to use the reduced performance levels for the capacity limit states. For the seismic designed building, the stiffness is much higher comparing to Structure 1, thus both yielding and ultimate deformation are increased comparing. Therefore, using the performance level of 1%, 2% and 4% accordingly will be appropriate for this structure.

From the pushover analysis it could also be found that the deformation of the first story is significantly larger than that of the second one, which is the same as the results of the previous nonlinear dynamic time history analysis.

3.7 Developing fragility curve

The development of fragility curves is an important part of this section. In this study, fragility is defined as the conditional probability of exceeding prescribed limit states written as equation 3-1. The limit state function in equation 3-1 is defined as follows

$$g(Sa;\boldsymbol{\Theta})=C-D(Sa;\boldsymbol{\Theta}) \tag{3-5}$$

In this equation, C stands for the capacity while D is the demand given the value of Sa.

Fragility curve can be constructed using the probabilistic demand model developed in section 3.5 and the capacity limit states obtained in section 3.6. When equation 3-2 is used in this research, σ_M and σ_C are assumed to be equal to 0.3 (Wen et al. 2004) and σ_D equals σ obtained from the bilinear demand model.

As a result of the bilinear demand model used in section 3.5, the change in demand model will cause a jump in the fragility curve. The change is mainly due to relatively larger σ_D value in the inelastic range of the demand model. In order to obtain a continuous fragility curve, a lognormal function is used to obtain the fragility curve in the entire Sa range (Ramamoorthy et al., 2006). The lognormal function is

$$\hat{F}(Sa;\boldsymbol{\Gamma})=\Phi\left(\frac{\ln(Sa)-\gamma_1}{\gamma_2}\right) \tag{3-6}$$

where $\boldsymbol{\Gamma}=(\gamma_1,\gamma_2)$ which represent the unknown parameters of the lognormal distribution. The parameters can be obtained by fitting the new lognormal fragility curve on the original discontinuous fragility curve as shown in Figure 3-18 in which the fragility curves of Structure 1 for the pushover performance levels are developed as an example. It could be noted that the Sa

value only reaches 1.2g in this figure for a better illustration of the method and a complete fragility curve plot will be given in latter figures.

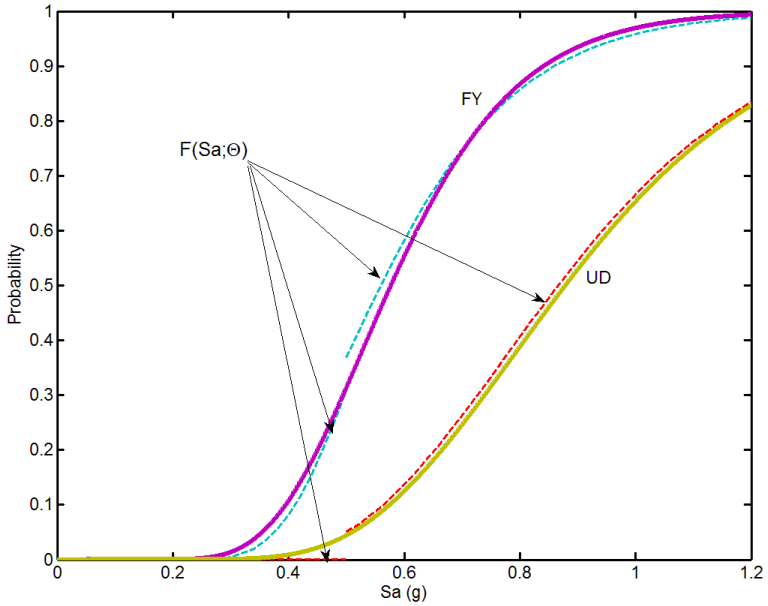

Figure 3.18 Fragility Estimate for Structure 1 Using the Pushover Performance Levels

In Figure 3.19, the fragility curves for the structure designed with gravity loads only (Structure 1) were exhibited based on both FEMA and pushover performance levels.

Similarly to Figure 3.19, the fragility curves for the structure designed considering the earthquake loads (Structure 2) were shown on both FEMA and pushover performance levels in Figure 3.20.

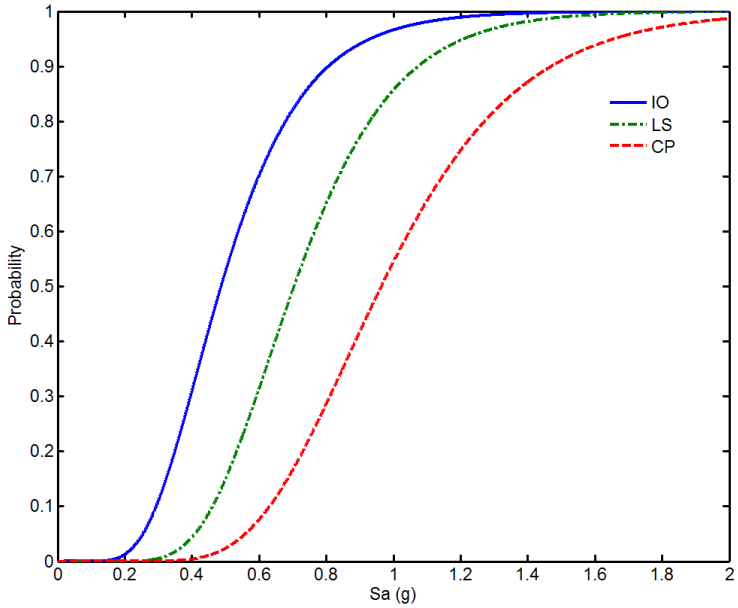

a) FEMA performance levels

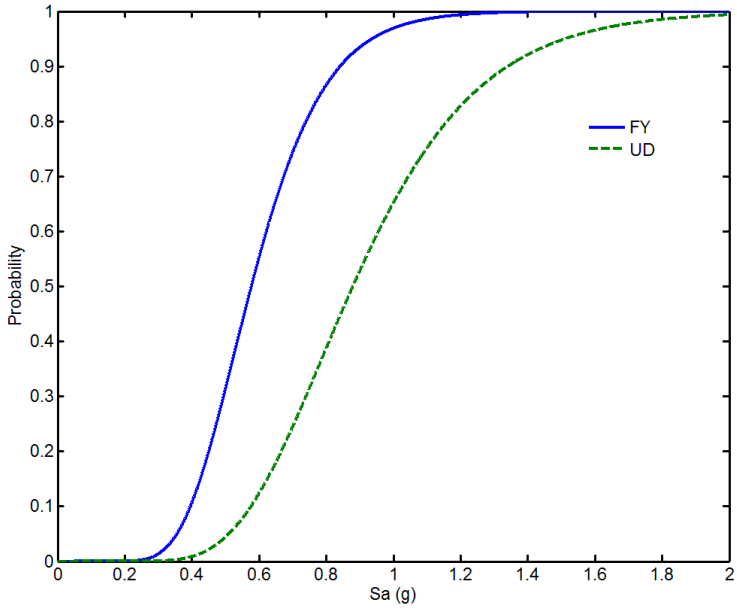

b) Pushover performance levels

Figure 3.19 Fragility Estimates for Structure 1

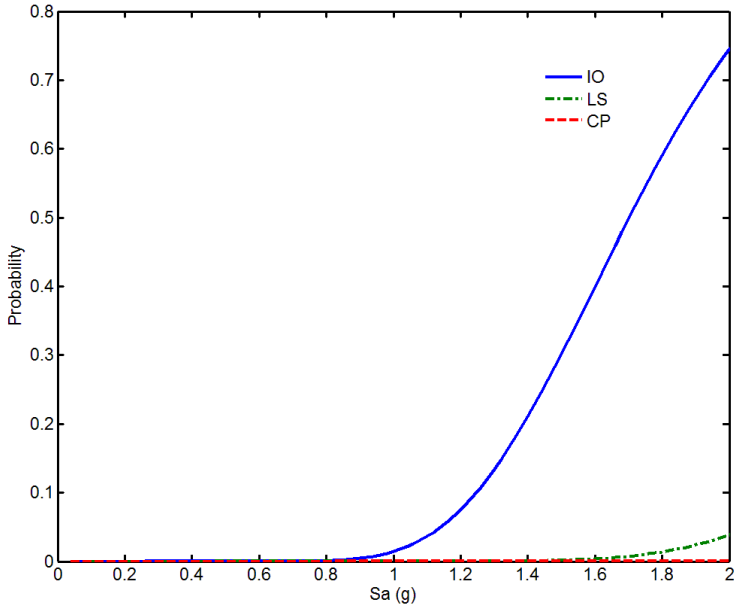

a) FEMA performance levels

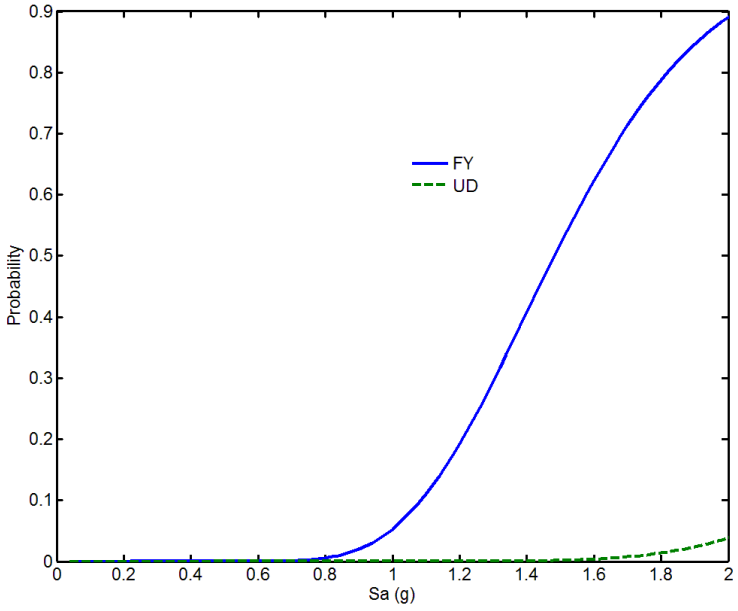

b) Pushover performance levels

Figure 3.20 Fragility Estimates for Structure 2

From the above figures it could be found that the probability of exceeding certain performance levels is significantly smaller in Structure 1 than in Structure 2 under the same Sa values. For a realistic Sa range, the probability of collapse or even experiencing heavy damage is close to 0 for Structure 2 which indicating the necessity of seismic design. For Structure 1, the probability of collapse is relatively large even under a moderate Sa value. Therefore, it could be understood that those pre-code structures will be the main source of structural damage in damaging earthquakes. It could also be noted that although the Sa value for all plots reaches 2.0 g in all fragility curves, the confidence interval is only up to about 1.7 g which corresponds to the maximum Sa value obtained in the virtual experiments in section 3.5.

3.8 Fragility estimate using story specific demand model

In order to verify the accuracy of the fragility curves obtained in section 3.7, the story specific model proposed by Bai, Gardoni and Hueste (2010) is also used for developing the fragility curve of the building designed with gravity loads only (Structure 1).

The same Bayesian updating rule will be used for an independent regression analysis for two sets of data independently at first. Then another bivariate demand model will be developed based on the mythology proposed by Gardoni (2002) for the bivariate capacity model in which the unknown coefficient of correlation ρ will be introduced in.

When the two demand models are developed separately, the results are shown in Figure 3.21 and the parameters are shown in Table 3.13. It could be noted that for the second story, the inter-story drift ratio δ is relatively small and all the data are type 1 data defined in Chapter 3.

Therefore, a single liner model is used for this story while the more accurate bilinear model is used for the first story.

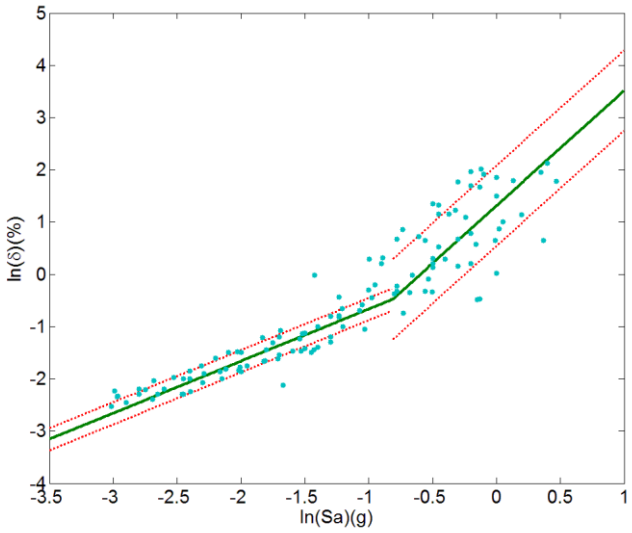

a) Story 1

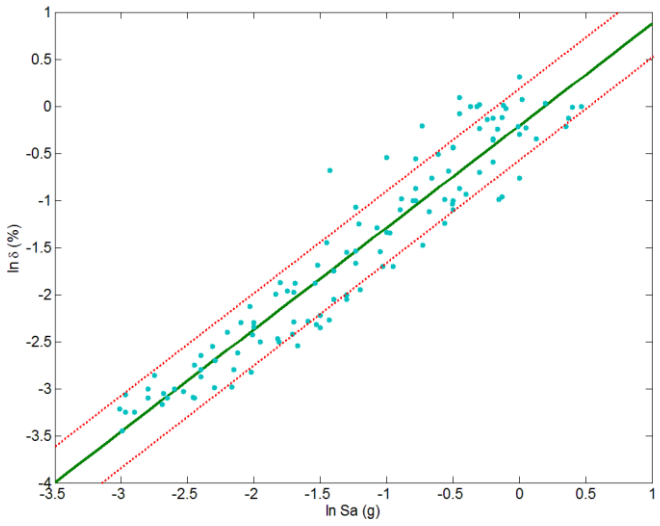

b) Story 2

Figure 3.21 Story Specified Probabilistic Demand Model for the Example Structure

Table 3.13 Posterior Statistics of Unknown Parameters in the Demand Model for the Sample Structure

Range	Parameter	Mean	Standard deviation	Correlation Coefficient		
				θ_0	θ_1	σ
Story 1 $\delta < \delta 1$	θ_0	0.3292	0.038	1	0.98	−0.01
	θ_1	0.9963	0.021	0.98	1	0.01
	σ	0.2130	0.007	−0.01	0.01	1
Story 1 $\delta > \delta 1$	θ_1	2.2057	0.115	NA	1	0.35
	σ	0.7692	0.068	NA	0.35	1
Story 2	θ_0	−0.2059	0.023	1	0.97	−0.03
	θ_1	1.0830	0.021	0.97	1	0.02
	σ	0.3311	0.012	−0.03	0.02	1

When a bivariate demand model is developed instead of the previous independently developed demand model for each story, the posterior statistics of relevant parameters are shown in Table 3.14.

Table 3.14 Posterior Statistics of Unknown Parameters in the Bivariate Demand Model for the Sample Structure

Range	Parameter	Mean	Standard deviation	Correlation Coefficient						
				θ_0	θ_1	σ	θ_0	θ_1	σ	ρ
Story 1 $\delta < \delta 1$	θ_0	0.4492	0.052	1						
	θ_1	1.0237	0.027	0.98	1					
	σ	0.215	0.007	−0.07	0.10	1				
Story 2 Part 1	θ_0	−0.3838	0.032	0.02	−0.09	0.00	1			
	θ_1	1.0054	0.025	0.01	0.06	−0.01	0.97	1		
	σ	0.2894	0.012	0.03	0.02	0.02	−0.01	0.01	1	
	ρ	0.733	0.013	0.01	0.01	−0.03	−0.02	−0.03	−0.03	1
Story 1 $\delta > \delta 1$	θ_0	1.2957	0.032	1						
	θ_1	1.7980	0.127	0.86	1					
	σ	0.7701	0.016	−0.02	−0.17	1				
Story 2 Part 2	θ_0	−0.3556	0.035	0.01	−0.04	0.00	1			
	θ_1	1.1520	0.029	0.02	−0.03	0.02	0.99	1		
	σ	0.4012	0.008	0.02	−0.03	0.18	−0.04	−0.08	1	
	ρ	0.401	0.017	0.00	0.02	−0.01	−0.02	−0.02	−0.02	1

From the table it could be observed that the mean values and standard deviations for the relevant parameters are nearly the same as the corresponding estimates in the individual model listed in Table 3.14.

Based on the bivariate fragility estimate mythology proposed by Choe, Gardoni and Rosowsky (2007), the fragility can be computed using the equation:

$$F(Sa;\boldsymbol{\Theta}) = 1 - \Phi_2(\mathbf{u}, \hat{\mathbf{R}}) \tag{3-7}$$

Where $\mathbf{u}$ is vector of parameters related to Both demand and capacity and $\hat{\mathbf{R}}$ is the estimated correlation coefficient matrix. For the evaluation of $\Phi_2(\mathbf{u}, \hat{\mathbf{R}})$, the numerical expression could be obtained following the method of Ambartzumian et al. (1998).

$$\Phi_2(u_1, u_2, \hat{\rho}) = \Phi(u_1)\Phi(u_2) + \int_0^{\hat{\rho}} \varphi_2(u_1, u_2, \hat{\rho}) d\hat{\rho} \tag{3-8}$$

The above equation can be easily solved numerically. Then the new fragility can be developed and the same capacity limit state will be used. For the purpose of comparison, only the FEMA performance limit states will be used in this case and the resulting fragility curve is plotted in Figure 3.22.

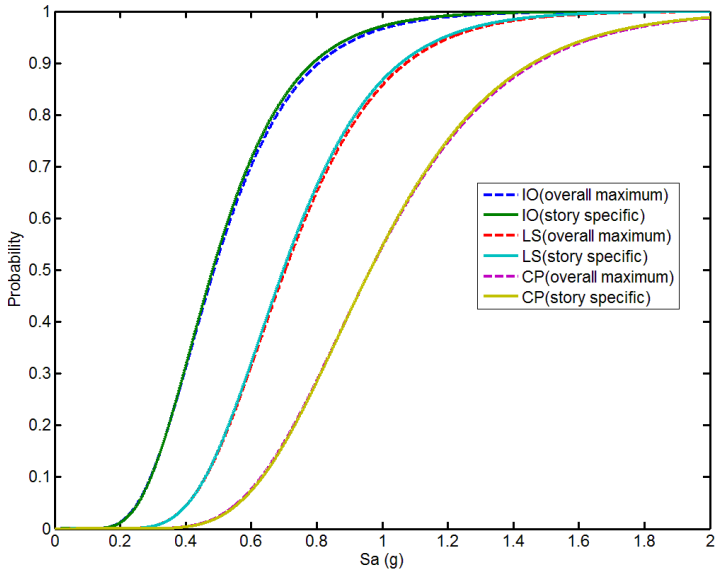

Figure 3.22 Fragility Estimate Using Story Specific Demand Model

The story specific demand model provides almost the same result as the ordinary bilinear demand model using the overall maximum interstory drift ratio as indicated in Figure 3.22. A possible explanation for the result is that the first story behavior dominates in this two story building. Therefore, it would be better to use a story specific model when the building has more stories and the overall performance is more complex. For the case of this two story building, using the overall maximum inter-story drift ratio model will be accurate enough to provide the fragility estimate.

3.9 Conclusions

In this section, the fragility curves for two buildings were constructed. The first structure (Structure 1) is designed for gravity loads only represents pre-code structure in the earthquake region while the second structure is designed in consideration of the earthquake loading. Five bins of ground motion records were selected for the construction of a bilinear probabilistic demand model based on the mythology proposed by Gardoni et al. (2002). The data points were obtained using a large number of non-linear dynamic time history analysis. The probability capacity model is based on both FEMA 356 performance levels and performance levels obtained from the pushover analysis. Fragility curves were then developed using the mythology of Ramamoorthy et al., 2006 on the basis of both demand and capacity models. In the final part, the story specific demand model is used to construct the same fragility curve, the similarity in the curves indicated that the overall maximum interstory drift model will be sufficient for the purpose of the sample two story building used in this study.

CHAPTER 4

SEISMIC DEGRADATION OF THE STRUCTURE AND ITS INFLUENCE ON THE FRAGILITY CURVE

4.1 Introduction

In current seismic codes, buildings are designed for one-time earthquake without considering the effect of multiple earthquakes. In the research of seismic fragility, most current researches are also based on the as built condition of the structure. It is true that most major damages come with the main shock or first earthquake but some most recent examples have shown that the aftershocks or multiple earthquakes can also cause severe damage to the already damaged buildings, thus leading to economical loss. Therefore, it is important and necessary to include the effect of multiple earthquakes in the developing of fragility curves.

In this chapter, the fragility curve of first earthquake damaged buildings will be constructed based on the degradation model for RC columns proposed by Kumar and Gardoni (2012) and the change of capacity model will also be considered. For the degradation of pushover properties, properties such as stiffness, deformation at yield and shear force at yield will be considered since these properties will have a large influence on the seismic performance of the structure. . For the change of capacity, new pushover analyses will be conducted using the degraded pushover properties.

With the column degradation model of Kumar and Gardoni (2012), it is able to construct the degradation model for the whole structure by treating each column separately. Therefore, the degradation of properties of each column could be obtained using a story specified demand model in section 3.8 to represent the previous earthquake without knowing the actual earthquake ground

motion of it. Afterwards, by conducting the same analysis process in the previous chapter, the new fragility curve of the whole structure can be obtained for different Sa values of the first earthquake.

4.2 Degradation of pushover properties of RC columns

For the purpose of this study, pushover properties considered are the lateral stiffness (K) and the yield point (Δ_y , V_y). The relationship between these three parameters are K= V_y / Δ_y . Therefore, modeling any two properties will be enough for the modeling of the degradation of the columns. A linear probabilistic model is used to predict K/K' and Δ_y / Δ_y' in which the prime sign of K' and Δ_y' represents the state after the main shock. The expressions for the model is given as (Kumar and Gardoni, 2012)

$$\ln(K'/K) = [\sum_{i=1}^{n} \theta_{K,i} h_{K,i}(x)] \ln(\delta_D / \delta_y) + \sigma_K \varepsilon_K \qquad \delta_D / \delta_y > 1 \tag{4-1}$$

$$\ln(\Delta'_y / \Delta_y) = \theta_{\Delta,1} \ln(K'/K) + \sigma_\Delta \varepsilon_\Delta \qquad \delta_D / \delta_y > 1 \tag{4-2}$$

where $\theta_{K,i}$, $\theta_{\Delta,1}$, σ_K and σ_Δ are unknown model parameters and $h_{K,i}(x)$ are explanatory terms. ε_Δ and ε_K are both standard normal distributions and $h_{K,i}(x)$ are selected to represent the global behavior of RC columns and in this model. $h_{K,1}(x)$ is equal to constant value 1.0; $h_{K,3}(x) = P_u / (f'_c A_g)$ and $h_{K,3}(x) = T_n$. It could be noted that Pu is the axial load on the column due to both the self-weight of the column and the weight of super structure; f'c is the compressive strength of concrete and Ag is the gross cross sectional area of the column; The last term $T_n = 2\pi\sqrt{P_u / Kg}$ where K is the lateral stiffness of the column. It could be noted that in both

equation 4-3 and equation 4-4, the model is only for δ_D / δ_y >1 and the reason is that for $\delta_D / \delta_y \leq 1$, the column is theoretically in elastic range and the degradation of those pushover properties is ignored.

In Table 4.1, the posterior means and standard deviations of the unknown parameters in equation 4-1 and equation 4-2 are obtained using the Bayesian updating rule with a non-informative prior distribution by Kumar and Gardoni, 2012. The results will be used for the development of fragility curves in latter sections.

Table 4.1 Posterior Means and Standard Deviations of the Unknown Parameters in the Probabilistic Degradation Model

Parameters	$\theta_{K,1}$	$\theta_{K,2}$	$\theta_{K,3}$	$\theta_{\Delta,1}$	σ_{Δ}	σ_{K}
Mean	-0.735	0.347	0.124	-0.976	0.050	0.120
Standard Deviation	0.018	0.25	0.033	0.0029	0.005	0.0053

Results in Table 4.2 shows that the mean value for $\theta_{\Delta,1}$ is very close to -1, meaning that the value of V_y remained almost constant during the earthquake.

4.4 Development of fragility curves

Fragility curves are developed based on a similar mythology in chapter 3. For the consideration of one main shock and one aftershock, the seismic fragility can be written as follows conditioning on the spectral acceleration of the main shock and the aftershock:

$$\tilde{F}\left[S_a^1, S_a^2\right] = P\left\{C[S_a^1] - D[S_a^1, S_a^2] < 0 \middle| S_a^1, S_a^2\right\} \tag{4-3}$$

where, S^1_a is the spectral acceleration of the first earthquake and S^2_a is the spectral acceleration of the second earthquake. C and D represents the seismic capacity and demand accordingly. To better illustrate the process of developing the fragility curves for main shock damaged buildings, an example structure is used which is the same as the non-seismic designed building in Chapter 3.

Since the degradation model of both pushover properties and low-cycle fatigue damage are based on the value δ_D / δ_y. It is important to get the relationship between S_a and δ_D / δ_y for each column in the structure using a probabilistic demand model. Based on the fact that the structure is symmetric, the performances of columns in the same story are assumed to be the same.

The next step of the analysis will be calculating the degraded pushover properties in which equation 4.3 and 4.2 will be used. Afterwards, the new demand model will be constructed using the degraded properties obtained. The results are shown in Figure 4.1, Figure 4.2, Figure4.3 and Table 4.2. It could be noted that after the degradation, the natural periods of the structures would decrease and the new periods were decided by the eigenvalue analysis.

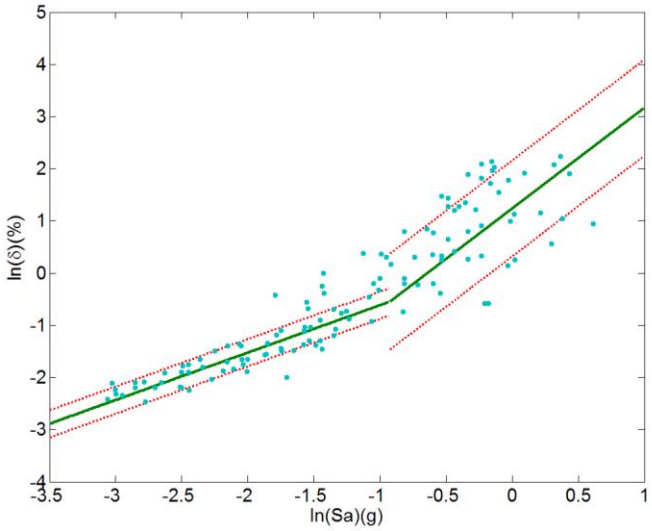

Figure 4.1 Probabilistic Demand Model for S_a^1=0.6g

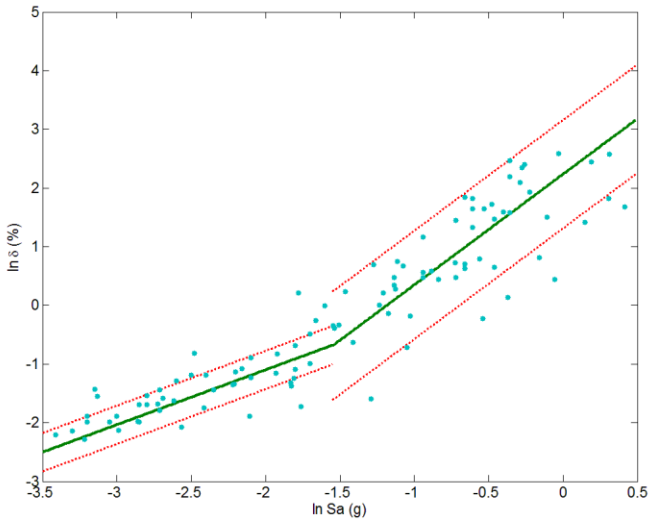

Figure 4.2 Probabilistic Demand Model for S_a^1=0.8g

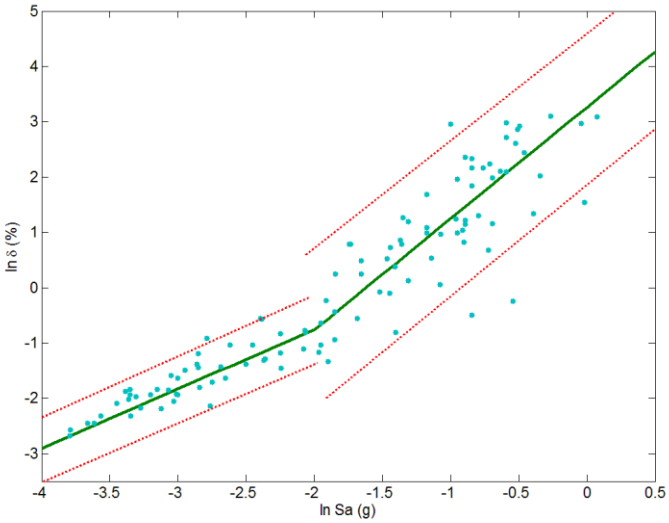

Figure 4.3 Probabilistic Demand Model for S_a^1=1.0g

Table 4.2 Posterior Statistics of Unknown Parameters in the Demand Model for the Damaged Structures

S_a[1]	Range	Parameter	Mean	Standard deviation	Correlation Coefficient		
					θ_0	θ_1	σ
0.6g	$\delta < \delta 1$	θ_0	0.2914	0.033	1	0.98	−0.05
		θ_1	0.9087	0.022	0.98	1	0.02
		σ	0.2612	0.007	−0.05	0.02	1
	$\delta > \delta 1$	θ_1	1.9303	0.102	NA	1	0.31
		σ	0.9201	0.088	NA	0.31	1
0.8g	$\delta < \delta 1$	θ_0	0.7708	0.062	1	0.96	−0.02
		θ_1	0.9354	0.024	0.96	1	0.01
		σ	0.3276	0.011	−0.02	0.01	1
	$\delta > \delta 1$	θ_1	1.8873	0.121	NA	1	0.43
		σ	0.9231	0.081	NA	0.43	1
1.0g	$\delta < \delta 1$	θ_0	1.3903	0.091	1	0.99	−0.02
		θ_1	1.0741	0.022	0.99	1	0.00
		σ	0.3512	0.013	−0.02	0.00	1
	$\delta > \delta 1$	θ_1	2.0127	0.133	NA	1	0.51
		σ	0.9746	0.082	NA	0.51	1

For the seismic capacity, the pushover performance levels for are used on the basis of nonlinear pushover analysis with the buildings of degraded pushover properties. The resulting pushover curves are plotted in Figure 4.3. For the FEMA limit states, no change will be made to the capacity limit state values. The resulting new pushover capacity limit states are given in Table 4.3.

Table 4.3 Yielding and Ultimate Maximum Interstory Drift Ratio of Degraded Structures

Structure Type	Yielding δ (%)	Ultimate δ (%)
Original	0.62	1.60
S_a^1=0.6g	0.58	1.55
S_a^1=0.8g	0.51	1.42
S_a^1=1.0g	0.49	1.40

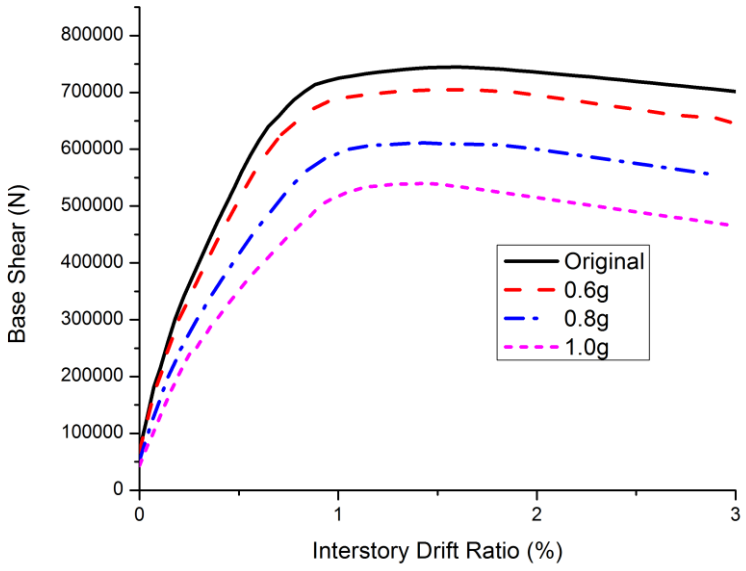

Figure 4.4 Pushover Analysis for Damaged Buildings

After getting both the seismic demand and capacity model, the fragility of the damaged structure can be obtained using the same method in Chapter 3. The fragility curves are developed considering the degradation of the seismic capacity discussed above. Fragility curves of both undamaged and damaged buildings are developed and compared in Figure 4.5 and Figure 4.6.

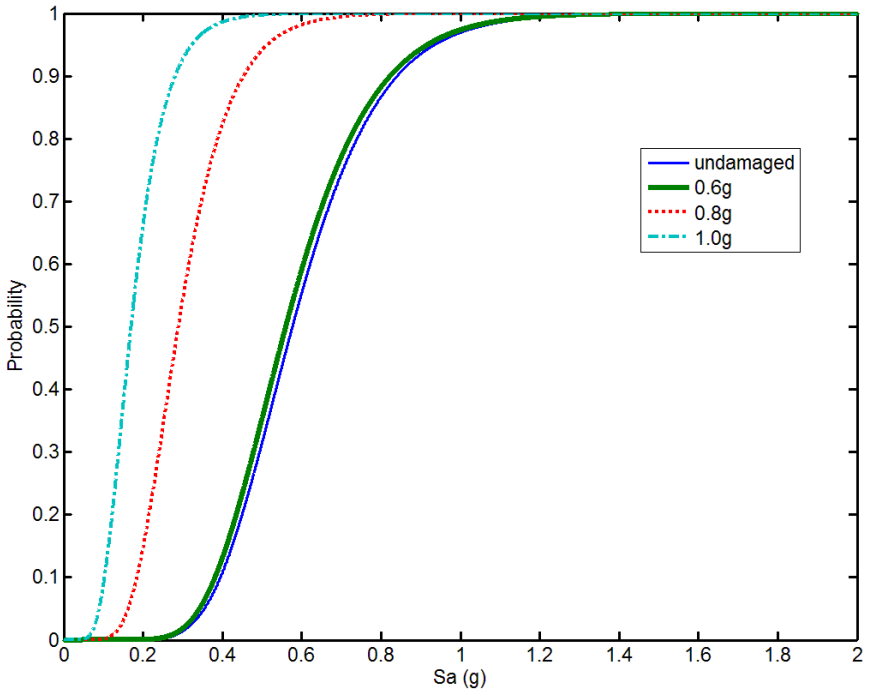

Figure 4.5 Fragility of Damaged Buildings for First Yield (FY)

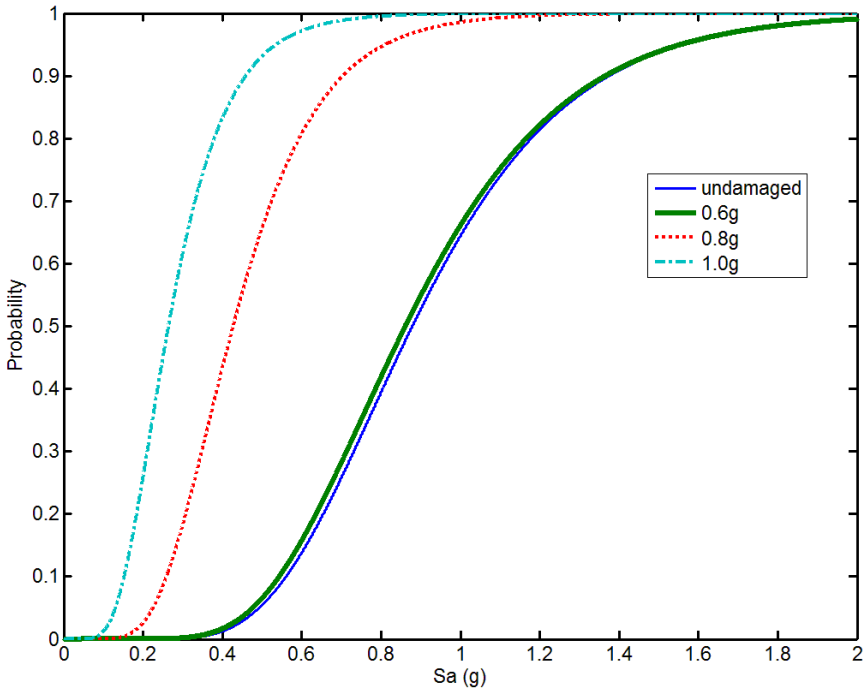

Figure 4.6 Fragility of Damaged Buildings for Ultimate Deformation (UD)

Figure 4.5 and Figure 4.6 show that the fragility increases with the increasing spectral acceleration of the first earthquake. When the first earthquake is relatively small, the increase of fragility is not obvious but after a large main shock, the fragility increases significantly. For a main shock of 1.0 g, the probability of exceeding the ultimate deformation performance level is relatively high even at small values of Spectral acceleration. Therefore, it becomes important to re-estimate the fragility of the structure after the main shock to ensure an accurate prediction of the fragility of the RC structure. It should also be noted that similar to the fragility curves in Chapter 3, the curves are accurate only to 1.7g based on the Sa range of the virtual experiment results.

Using the same mythology, the fragility of other conventional low rise multi-story RC buildings can be calculated for considering multiple earthquake effects in the service life.

4.5 Conclusions

In this chapter, the fragility curves of damaged structures were constructed and compared with the fragility curves of the undamaged structure. In order to construct the fragility curves, the seismic degradation model of static pushover properties were used since the pushover properties such as lateral stiffness and yielding point are critical to the seismic performance of a structure. In addition, the change of deformation capacity was also considered and calculated by performing nonlinear time history analysis on the damaged structure.

Based on the degradation of both static pushover properties and deformation capacity, the fragility curves were constructed using the same mythology in Chapter 3. A sample structure was used for the analysis to illustrate the process and the story specified demand model from Chapter 3 was used for the computation of degraded static pushover properties. According to the resulting fragility estimates, the degradation caused by the first earthquake will cause significant increase in the seismic fragility of the building. The proposed method could be used more generally to evaluate the fragility of low rise multi-story RC structures.

CHAPTER 5
SUMMARY AND CONCLUSIONS

5.1 Summary

Increasing the earthquake performance of structures is critical for reducing the overall loss caused by the earthquake. Therefore, the accurate estimation of seismic fragility of a structure becomes important. The damage of the structure during an earthquake is mainly caused by the first earthquake, but the influence of the multiple earthquakes during the service life cannot be ignored based on some most current examples.

This research focuses on the development of fragility curves of main shock damaged structures. The probabilistic degradation model of RC columns for both static pushover properties proposed by Kumar and Gardoni, 2012 is the foundation of the mythology for estimating the fragility of a degraded structure in this study. By applying the degradation model of a single column to the whole structural system, we proposed a mythology to evaluate the fragility of mainshock damaged structure. By using this mythology, the fragility is evaluated using both the first earthquake and the earthquakes afterwards which could give a more accurate estimation of the fragility for buildings during the entire service life, thus providing help for the decision making after earthquake hits.

5.2 Concluding remarks

The main conclusions and contributions made in this thesis are as follows:

Firstly, the probability of the occurrence of aftershocks in a main shock-aftershock sequence is computed using the modified Omori's law. A sample calculation is carried out for the California region showing that the probability of a damaging aftershock is relatively high in a short time span after the mainshock and the influence of the aftershock should not be ignored in the fragility analysis of structures. This study gives the lower bound of the probability of multiple earthquakes since main shock aftershock sequence is a special case of multiple earthquake effects.

Secondly, two sample structures are used for the construction of fragility curves of undamaged structures. In order to count for the uncertainties within the analysis, 5 bins of earthquake ground motion records are selected based on both magnitude and closest distance from the source. The demand model is obtained using a Monte Carlo simulation and a bilinear model is used for the construction of the model. The capacity limit states used in the analysis are from both FEMA performance levels and pushover analysis performance levels. After constructing the fragility curves, it could be found that the fragility of the structure designed with gravity loads only is much higher than that of the structure designed in consideration of the earthquake loads. For verifying the fragility estimates, the bivariate story specific demand model is also used. The result indicates that the overall maximum drift ratio demand model will be accurate enough for the two story sample building but the story specific model should be used when the number of stories increases.

The third and most important part of this study is to propose a mythology for developing fragility estimates of damaged structures. The degradation model proposed by Kumar and Gardoni, 2012 for RC columns are used in this study for static pushover properties. The story specified demand model is used for the computation of the degradation model since columns in each story are different in both properties and performances during the main shock. A sample structure is used

for the explanation of the mythology and the mythology provides a general method to estimate the fragility of low rise multi-story structures under multiple earthquake effects in the service life.

5.3 Suggestions for Future Work

There are some updates could be done for the mythology used in this study.

1. The degradation model by Kumar and Gardoni, 2012 is developed mainly for bridge columns. Therefore, developing a specified model for structure columns will provide a more accurate result for the analysis.
2. Only the degradation of pushover properties of columns is considered in this research. Therefore, more modification could be made to the mythology by introducing a model for degradation of connections, beams and even nonstructural components.
3. Only two earthquakes are considered in the mythology and updates can be made to include the effect of multiple earthquakes, for example a series of aftershocks or more than two earthquakes during the service life.

REFERENCES

Abramhamson, N. A., and Silva, W. J. (1997). Empirical response spectral attenuation relations for shallow crustal earthquakes. *Seismological. Research Letters*, 68(1), 94–127.

ACI. (2005). Building code requirements for structural concrete and commentary. ACI-318, American Concrete Institute, Farmington Hills, Mich.

Ambartzumian, R. V., Kiureghian, A., Oganian, V. K., and Sukiasian, H.S. (1998). Multinormal probability by sequential conditioned importance sampling: Theory and application. *Probab. Eng. Mech.*, 13(4), 299–305.

Baker, J. W., and Cornell, C. A. (2008). Vector-valued measures for pulse-like near-fault ground motions. *Eng. Struct.*, 30(4), 1048–1057.

Box, G. E. P., and Tiao, G. C. (1992). Bayesian inference in statistical analysis, Addison-Wesley, Reading, Mass.

Bai,J.W., Gardoni, P. and Hueste, M. B. D.(2011). Story-specific demand models and seismic fragility estimates for multi-story buildings. *Structural Safety*, 33, 96–107

Choe, D.E.; Gardoni, P., and Rosowsky, D. (2007). Closed-form fragility estimates, parameter sensitivity, and Bayesian updating for RC columns. *Journal of Engineering Mechanics*, 133(7), 833-843

Choe, D., Gardoni, P., Rosowsky, D., and Haukaas, T. (2009). Seismic Fragility Esti-mates for Reinforced Concrete Bridges subject to Corrosion. *Structural Safety*, 31(4), 275-283.

Elnashai, A., & Di Sarno, L. (2008). Fundamentals of earthquake engineering. John Wiley & Sons Ltd, London, UK.

Elnashai A.S., Papanikolaou V., Lee D.H.(2002) ZEUS-NL user manual: Mid-America earthquake center. University of Illinois at Urbana-Champaign, Urbana, IL.

FEMA. (2000). Pre-standard and commentary for the seismic rehabilitation of buildings. Rep. No. FEMA-356, Federal Emergency Management Agency, Washington, D.C.

Gardoni, P., Der Kiureghian, A., and Mosalam, K. M. (2002). Probabilistic capacity models and fragility estimates for RC columns based on experimental observations. *J. Eng. Mech.*, 128(10), 1024–1038.

Gardoni, P., Mosalam, K. M., and Der Kiureghian, A. (2003). "Probabilistic seismic demand models and fragility estimates for RC bridges. *Journal of Earthquake Engineering*, 7(1), 79–106.

Hatzigeorgiou, G.D. and Liolios, A.A. (2010). Nonlinear behavior of RC frames under repeated strong ground motions. *Soil Dynamics and Earthquake Engineering*. 30(10), 1010-1025.

Hwang, H.H.M., and Huo, J-R. (1994). Generation of hazard consistent fragility curves. *Soil Dynamics and Earthquake Engineering*, 13, 345-354.

Hwang, H. H. M., and Jaw, J. W. (1990). Probabilistic damage analysis of structures. *J. Struct. Eng*., 116(7), 1992–2007.

IBC (2009). International Building Code. IBC-2009, International Code Council, USA

Ji.J. (2007). Seismic fragility assessment of reinforced concrete high rise buildings. Ph.D. thesis, University of Illinois at Urbana-Champaign, Urbana, IL.

Lee, K., Foutch, D.A.(2004). Performance evaluation of damaged steel frame buildings subjected to seismic loads. *Journal of Structural Engineering*, 130(4), 588-599.

Li, Q. and Ellingwood, B.R. (2007). Performance evaluation and damage assessment of steel frame buildings under main shock–aftershock earthquake sequences. *Earthquake engineering & structural dynamics*, 36(3), 405-427.

Luco, N., Bazzurro, P. and Cornell, C. A. (2004). Dynamic versus static computation of the residual capacity of a main shock-damaged building to withstand an aftershock. *13th World Conference on Earthquake Engineering*. Paper No. 2405.

Omori, F. (1984). On the aftershocks of earthquakes. *Journal of the College of Science*, 7(2), 111-200.

Ramamoorthy, S.K., Gardoni, P., and Bracci, J.M. (2006). Probabilistic demand models and fragility curves for reinforced concrete frames. *Journal of Structural Engineering*, 132(10), 1563-1572.

Ramamoorthy, S. K. (2006). Fragility estimates for reinforced concrete framed buildings. Ph.D. thesis, Texas A&M Univ., College Station, Tex.

Ramamoorthy S.K., Gardoni P, Bracci J.M.(2008). Seismic fragility and confidence bounds for gravity load designed reinforced concrete frames of varying height. *Journal of Structural Engineering*;134(4):639–650.

Reasenberg, P. A. and Jones, L. M. (1989), Earthquake Hazard after a Main Shock in California, Science 243(4895), 1173–1176.

Shome, N. (1999). Probabilistic seismic demand analysis of non-linear structures. Ph.D. thesis, Stanford University, Stanford, CA.

Shinozuka, M., Feng, M-Q., Lee, J., and Naganuma, T. (2000). Statistical analysis of fragility curves. *J. Eng. Mech*. 126(12), 1224-1231.

Smyrou, E., Tasiopoulou, P., Bal, İ.E., Gazetas, G. and Vintzileou, E. (2011). Structural and geotechnical aspects of the Christchurch (2011) and Darfield (2010) earthquakes In New Zealand. *Seventh National Conference on Earthquake Engineering*, Istanbul, Turkey.

Utsu, T. (1961), A Statistical Study on the Occurrence of Aftershocks, *Geophys. Mag*. 30, 521–605.

Wen, Y.K., Ellingwood, B. R., and Bracci, J. M. (2004). Vulnerability functions. Mid-America Earthquake Center, University of Illinois, *Technical Report* No. DS-4, Champaign, Illinois.

Wen, Y.K., Ellingwood, B. R., Veneziano, D. and Bracci, J. M.(2003). Uncertainty modeling in earthquake engineering. Mid-America Earthquake Center, University of Illinois, *Technical Report* No. FD-2, Champaign, Illinois.

Wen, Y. K., and Wu, C. L. (2001). "Uniform hazard motions for mid-America cities." *Earthquake Spectra*, 179(2), 359–383.